NATIONAL AERONAUTICS AND SPACE ADMINISTRATION

TECHNICAL REPORT
R-117

TURBULENT BOUNDARY-LAYER SEPARATION INDUCED BY FLARES ON CYLINDERS AT ZERO ANGLE OF ATTACK

By DONALD M. KUEHN

1961

For sale by the Superintendent of Documents, U.S. Government Printing Office, Washington 25, D.C. Yearly subscription, $15; foreign, $19; single copy price varies according to size -------- Price 40 cents

TECHNICAL REPORT R-117

TURBULENT BOUNDARY-LAYER SEPARATION INDUCED BY FLARES ON CYLINDERS AT ZERO ANGLE OF ATTACK

By DONALD M. KUEHN

Ames Research Center
Moffett Field, Calif.

TECHNICAL REPORT R–117

TURBULENT BOUNDARY-LAYER SEPARATION INDUCED BY FLARES ON CYLINDERS AT ZERO ANGLE OF ATTACK

By Donald M. Kuehn

SUMMARY

Boundary-layer separation induced by a flare on a cylindrical body of revolution has been experimentally investigated in the Mach number range of 1.5 to 5.0 and in the Reynolds number range (based on boundary-layer thickness) of 1.50×10^4 to 12×10^4. Two flare types investigated were the compression corner and the curved surface. Three nose shapes were included: a 20° sharp cone, a 45° blunted cone, and a hemisphere. The purpose of the investigation was to determine the model geometry and flow conditions for which separation could be expected for a turbulent boundary layer on a cylinder-flare configuration. Comparisons were made of the boundary-layer-separation characteristics of these three-dimensional flares with two-dimensional separation results from a previous investigation.

The results showed that the variables which were important to two-dimensional boundary-layer separation were also important for the cylinder-flares. The tendency toward separation decreased for both the two- and three-dimensional models as Mach number was increased, and as Reynolds number, pressure rise, and pressure gradient were decreased. The pressure rise necessary to cause separation at the three-dimensional compression corner, for a given Mach number and Reynolds number, was found to be either equal to or greater than that for the two-dimensional models. Cylinder-flare models with large ratios of cylinder diameter to boundary-layer thickness were more prone to boundary-layer separation than configurations with small values of this ratio. Heat transfer into the model surface reduced the tendency toward separation. Changes in nose shape, unit Reynolds number, method of promoting transition, and length of cylindrical portion of the model had no influence on the first occurrence of separation at the flare. Conditions for incipient separation on blunt- and sharp-nosed models correlated on the basis of either free-stream conditions or boundary-layer-edge conditions. The latter correlation shows that flare-induced separation on a blunt-nosed cylinder can be predicted from data for sharp-nosed cylinders where the free-stream Mach number for the latter is equal to the boundary-layer-edge Mach number for the former.

INTRODUCTION

Boundary-layer separation is of interest in many phases of aerodynamics. In some design problems the presence of separation is undesirable since aerodynamic performance is dependent on an attached boundary layer. Thermodynamic considerations may, however, encourage the use of separated regions to reduce local heat transfer. Information on the conditions which cause separation should, therefore, be available so that the occurrence of separation can be predicted. When separation does occur, flow characteristics, such as extent of separation, boundary-layer steadiness, pressure distribution, and heat transfer, should be known so that the designer can judge the acceptability or desirability of the separated boundary layer. Present theoretical analyses cannot be used to predict the occurrence of separation and are of very limited value in estimating the characteristics of the separated region. Consequently, experimental results must be relied upon almost entirely.

Two-dimensional boundary-layer separation has been studied by a number of investigators. Reports of some of these studies (refs. 1–9) contain data obtained for compression corners, curved surfaces, incident shocks, and forward- and rear-

ward-facing steps. These investigations all had one thing in common they were studies of boundary layers which were forced to separate from the model surface by an imposed adverse pressure gradient and an over-all pressure rise greater than that necessary for incipient separation. A good understanding of the general characteristics of the separated region has resulted. These investigations do not, however, give any indication of the conditions necessary for the first occurrence of separation. References 10 and 11 also present data on the separated boundary layer and, in addition, give a small amount of information on the pressure rise the boundary layer will tolerate before it will separate from the surface. Reference 12 presents the results of an investigation devoted entirely to the incipient-separation pressure rise for two-dimensional turbulent boundary layers.

The quantity of data available on boundary-layer separation for three-dimensional bodies is considerably less than for two-dimensional bodies. Reference 13 is a theoretical investigation, and reference 14 is an experimental investigation of the interaction of a plane wave and a cylindrical body of revolution. Many references present information on the over-all aerodynamic characteristics of cylinder-flare configurations, since this geometry has become of special interest for drag control and stability of missiles. Boundary-layer separation, if observed, was considered only with respect to its influence on these over-all characteristics. The occurrence of separation was, however, not predictable. An investigation of three-dimensional turbulent boundary-layer separation has, therefore, been initiated as an extension of the two-dimensional investigation reported in reference 12. The purpose of this investigation is to obtain an understanding of the conditions for which boundary-layer separation can be expected for a turbulent boundary layer on a cylinder-flare configuration. Separation phenomena for the three-dimensional flared-afterbody model and the two-dimensional deflection surface (ref. 12) will be compared to determine possible similarities. Any generalities which can be concluded as a result of similarities in the separation phenomena that exist between various body shapes will provide a better basis for application of existing data to body shapes for which no experimental data are available.

NOTATION

D	diameter of cylinder, in.
l	distance along the model measured from the cylinder-flare juncture, in.(minus upstream, plus downstream)
L	length of model or of model component, in.
M	Mach number (for sharp-nosed models $M_\infty = M_e$)
n	velocity profile parameter, $\frac{u}{u_\infty} = \left(\frac{y}{\delta}\right)^{1/n}$
p	pressure, psia
r	radius of the curved portion of the curved-surface model, in.
R	Reynolds number, $\frac{u\delta_0}{12\nu}$ (for sharp-nosed models $R_{\infty_{\delta_0}} = \mathrm{R}_{e_{\delta_0}}$)
S	approximate location of the separation point as determined from the shadowgraphs
u	velocity, ft/sec
x	distance along model measured from the nose-cylinder juncture, in.
y	distance from the model normal to the surface, in.
γ	ratio of specific heats, 1.4 for air
δ	boundary-layer thickness, in.
θ	wedge angle for the compression corner or curved surface, deg
μ	viscosity, lb sec/ft^2
ν	kinematic viscosity, $\frac{\mu}{\rho}$, ft^2/sec
ρ	density, lb sec^2/ft^4

SUBSCRIPTS

cyl	cylindrical section of the model
flare	flared portion of the model
incip	condition for incipient separation
e	boundary-layer edge
∞	free stream
0	location on the cylinder where the static pressure is first affected by the presence of the flare
1	location on the flare at which the static pressure is a maximum
t	total conditions, for example, $\frac{p}{p_t} = \left(1 + \frac{\gamma - 1}{2} M^2\right)^{-\frac{\gamma}{\gamma - 1}}$

APPARATUS AND TEST METHODS

WIND-TUNNEL DESCRIPTION

The tests were conducted in the Ames 1- by 3-Foot Supersonic Wind Tunnel No. 1 which is a continuous-operation, closed-circuit tunnel. The minimum supersonic Mach number is about 1.2 to 1.6 and the maximum is about 5.0 to 6.0, depending on the size of the model. The maximum stagnation pressure range is approximately 2 to 59 psia. The upper limit of stagnation pressure varies with Mach number and is less than 59 psia for Mach numbers less than 3. The Mach number and total pressure are continuously variable during tunnel operation.

MODELS AND PRESSURE MEASUREMENT

The basic configuration was a cylindrical body of revolution with a flared afterbody, sting mounted at zero angle of attack. The major portion of the data was obtained using a model with a cylinder diameter of 1.25 inches, cylinder length equal to 9 cylinder diameters, and a conical nose with a 20° included angle. The relatively long cylindrical section was dictated by the requirements discussed in the section "Comparison of Two-Dimensional and Three-Dimensional Boundary-Layer Separation." Compression-corner and curved-surface flares with various flare angles were used to evaluate the influence of flare angle and shape. In addition, several special models were employed to evaluate the influence of other variables. Dimensions and designations of all models are given in figures 1(a) and 1(b). The variables investigated with each compression-corner flare are also tabu-

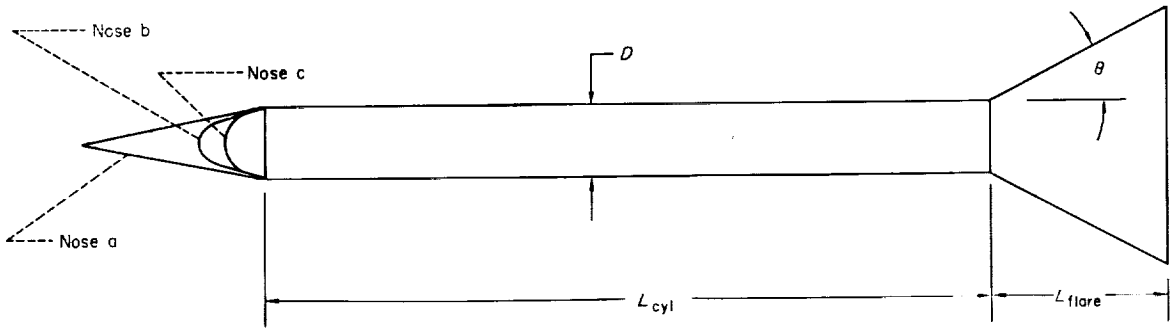

Model designation	D, in.	L_{cyl}/D	L_{flare}/D	Variables investigated with each model: Pressure rise, M, and θ	Nose shape	Method of promoting transition	L_{cyl}	R_∞	D/δ_o	Heat transfer	n not fully developed
[1]CC15-a-1	1.25	9	2.5	x							
CC20-a-1				x							
CC25-a-1				x							
CC25-a-3		4.2			x						x
CC25-c-3					x						x
CC30-a-0		9				x					
CC30-a-1				x	x	x			x		
CC30-a-2						x		x			
CC30-a-2-1	0.50		4.0					x			
CC30-a-2,3		29							x		
CC30-a-3	1.25	9	2.5			x					
CC30-a-3-1		4.2			x		x				x
CC30-b-1		9			x						
CC30-c-1							x				x
CC30-c-3		4.2			x		x				x
CC35-a-1		9		x							
CC35-a-2	0.35									x	

[1]CC, compression corner flare; 15, flare angle, θ; a, nose shape (fig. 1(c)); 1, method of promoting transition (fig. 1(d)). The flare is omitted for boundary-layer surveys; thus the designations are a-1, a-2, etc.

(a)

(a) Compression-corner models.

FIGURE 1.—Model geometry and designations.

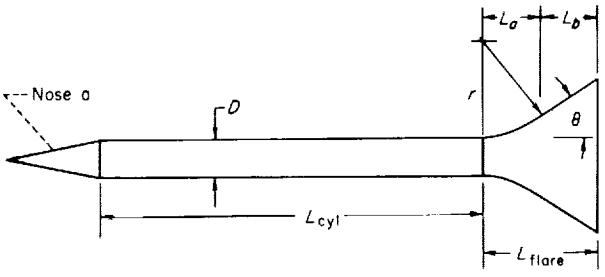

(b)

Model designation	D, in.	L_{cyl}/D	L_{flare}/D	r/D	L_a/D	L_b/D
CS25-a-1	1.25	9	2.5	2.6	1.10	1.40
CS35-a-1	↓	↓	↓	↓	1.49	1.01
CS45-a-1	↓	↓	↓	↓	1.84	0.66

(b) Curved-surface models.

FIGURE 1.—Continued.

lated in figure 1(a). Most models were instrumented with 0.0135-inch-diameter pressure orifices with a longitudinal spacing of 0.05 inch in regions where large pressure gradients were expected, and larger spacing in the regions of smaller expected pressure gradient. A solid copper model, mounted on an insulated sting, was used to evaluate the influence of heat transfer. This model contained a thermocouple located near the cylinder-flare juncture, but was not instrumented for pressure measurement.

Pressures were measured with a 150-inch multitube manometer board with a scale division of 0.1 inch. The manometer fluids were Dow-Corning silicone oil, tetrabromoethane, and mercury (respective specific gravities approximately 1, 3, 13.5). The lightest fluid permissible was always used to obtain maximum possible fluid deflection, and thus insure a maximum accuracy of pressure measurements. Pressures were obtained with a maximum error of 5 percent; however, the error generally was considerably less.

Boundary-layer trips.—Boundary-layer trips were used on most models to insure turbulent boundary layers over a larger Reynolds number range than would be possible if transition occurred naturally. The various methods of promoting

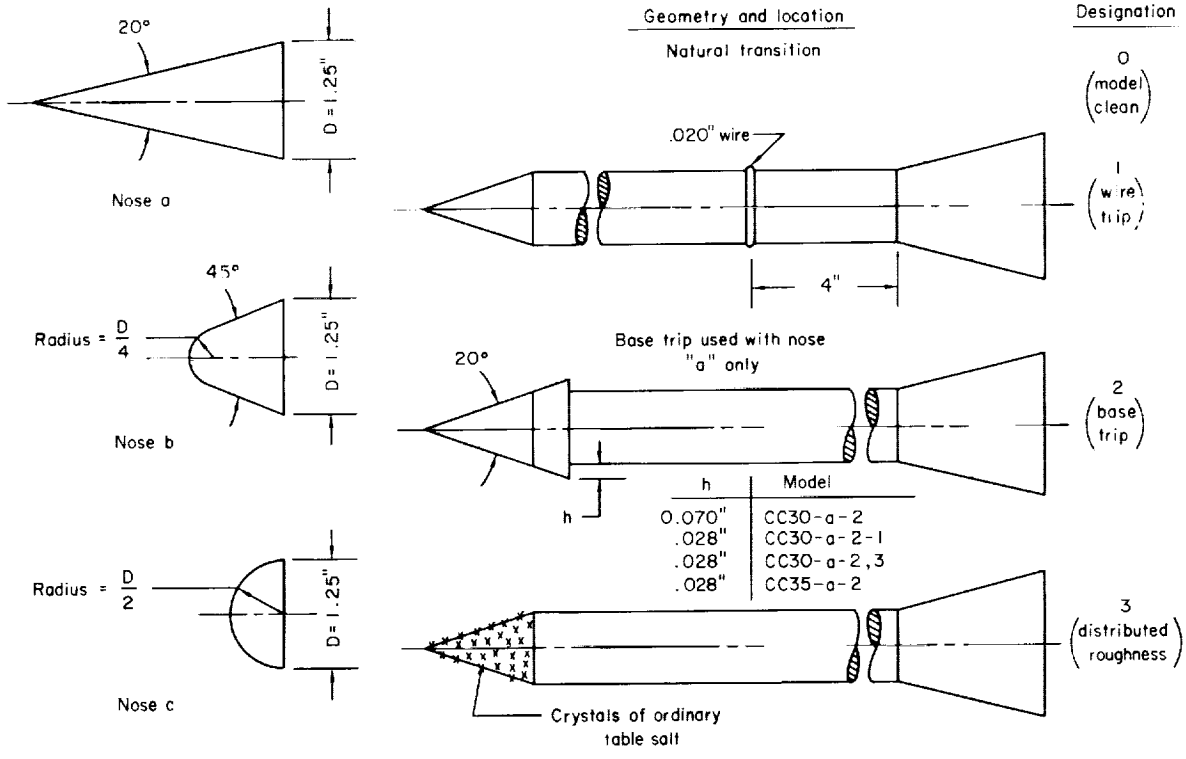

(c) (d)

(c) Nose shapes. (d) Boundary-layer trips; type and location.

FIGURE 1.—Concluded.

transition are shown in figure 1(d). For the purpose of assigning a designation, natural transition is also listed in this figure. The majority of the data for the model with cylinder diameter equal to 1.25 inches was obtained with a 0.020-inch wire trip located 4 inches ahead of the cylinder-flare juncture (trip 1). The size and location of the wire were dictated by boundary-layer-thickness requirements as discussed in the section "Comparison of Two-Dimensional and Three-Dimensional Boundary-Layer Separation." Other trips used were the base trip (trip 2) which was always located immediately behind the nose, and distributed roughness on the nose (trip 3) which consisted of crystals of ordinary table salt cemented to the model with lacquer

OPTICAL EQUIPMENT

For all test conditions the boundary layer and shock patterns were observed visually and were recorded by means of the shadowgraph technique. A continuous operation shadowgraph was used to view the flow field during the tests, and a spark shadowgraph with spark duration of about one microsecond was used to obtain photographic records of the flow. The mirror and the light sources were arranged so that nearly parallel light passed through the test section. A full-sized image was thus observed on a ground-glass screen mounted on the tunnel window opposite the light source. The ground-glass screen was replaced with a Polaroid-Land film pack when photographs were desired.

BOUNDARY-LAYER SURVEYS

Boundary-layer thickness was determined by pitot pressure surveys on all models except the heat-transfer model. The boundary-layer probe was made from 1/32-inch diameter steel tubing flattened to a nearly-rectangular opening approximately 0.004 inch high and 0.025 inch wide. The wall thickness was honed to approximately 0.002 inch. During a survey the probe tip moved perpendicular to the model surface and its position relative to the surface was indicated by a counter reading obtained from a previous calibration. The probe tip could be positioned at any desired longitudinal station on the body.

Boundary-layer profiles were obtained at two longitudinal stations in the region of initial pressure rise associated with the flare on models identical to those shown in figure 1, except that the flares were removed. This permitted surveys to be made without interference from the flare. Mach number and velocity profiles were obtained from the ratio of local static pressure on the model to the pitot pressure.

Boundary-layer thickness, δ, and velocity-profile parameter, n, were determined from log plots of u versus y as shown in figure 2. For the

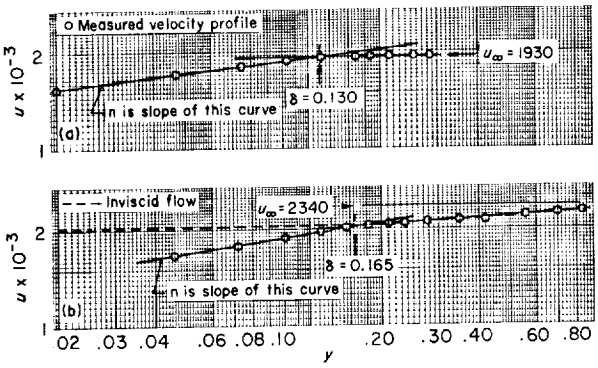

(a) Sharp-nosed models.

(b) Blunt-nosed models; shear-layer thickness $>> \delta$.

FIGURE 2.—Boundary-layer thickness.

sharp-nosed models, δ is simply the value of y where u deviates from u_∞. (See fig. 2(a).) This value of y was determined by the intersection of the straight line through the points representing velocities within the boundary layer and the straight line through the points representing free-stream velocity. Values of δ determined in this manner agreed with δ values determined from plots of M versus y, where δ was taken to be the value of y at $M=0.99\ M_\infty$. The blunt-nosed models are enveloped in a layer of variable-entropy air. The thickness of a boundary layer which is completely submerged in this shear layer should be the value of y at which the viscous velocity profile first deviates from the inviscid shear-layer profile. The computed inviscid velocity profile is represented by the smooth dashed curve shown in figure 2(b). The viscous and inviscid profiles coincide in the outer portion of the layer. As the surface is approached, however, the viscous profile breaks sharply from the inviscid profile as a result of the velocity reduction within the boundary layer. These viscous velocity profiles could generally be represented by two straight lines. The boundary-layer thickness for these models was, therefore, defined as the value of y where the viscous velocity curve changes slope. The

velocity profile parameters obtained from the velocity profiles are presented later in the report and are discussed with respect to whether the turbulent boundary layer was fully developed for the blunt models and the short models. Unless noted to the contrary, the boundary layers for all data presented had fully developed profiles.

METHOD OF DETERMINING INCIPIENT-SEPARATION CONDITIONS

The criterion used to detect the presence of a separated region in this investigation was identical to that established and discussed in reference 12; namely, the first appearance of a hump in the longitudinal pressure distribution (i.e., a pressure-distribution curve with three inflection points) marked the approximate onset of boundary-layer separation. The pressure rise for incipient separation was, therefore, defined as the over-all pressure rise which existed just before the first appearance of the hump.

Typical pressure distributions used to determine the test conditions at which the hump first appeared are shown in figure 3. Pressure rise

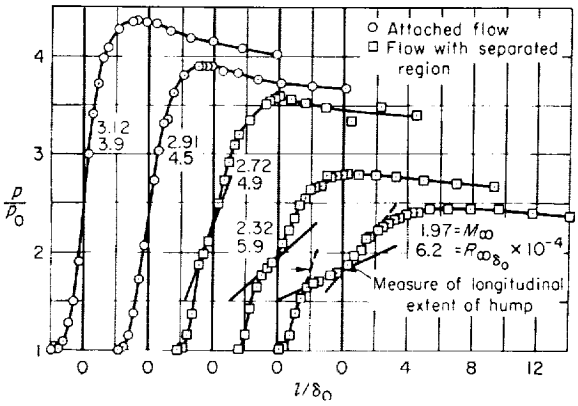

FIGURE 3.—Pressure distributions illustrating the occurrence of separation as Mach number is varied at a constant stagnation pressure; CC25 a 1.

above the undisturbed static pressure was plotted as a function of a dimensionless distance, l/δ_0. The pressure distributions were obtained with model geometry and stagnation pressure held constant as Mach number was varied from 3.12 (no separation) to 1.97 (sizable separated region). To determine the Mach number at which separation was incipient (between M_∞=2.72 and 2.91) a measure of the longitudinal extent of the hump in the pressure distribution was obtained (see fig. 3) as a function of Mach number and was extrapolated to zero. In spite of the fact that the size of hump in the pressure distribution was difficult to define accurately, the extrapolation was fairly accurate because the Mach number increments were small. Often the extrapolated Mach number was the same as that for which the first fully attached flow was observed, as was the case in figure 3. Separation was incipient at M_∞=2.91. Similar data were obtained for other values of stagnation pressure so the influence of Reynolds number on the Mach number for incipient separation could be established for each model geometry. Such data will then give the basic curve of incipient-separation conditions for a particular geometry as shown in figure 4.

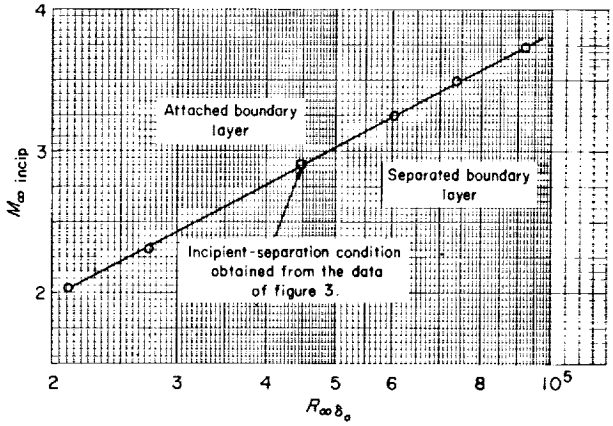

FIGURE 4.—Incipient separation data for the 25° flare; CC25 a 1.

RESULTS AND DISCUSSION PERTAINING TO THREE-DIMENSIONAL BOUNDARY-LAYER SEPARATION

The results of the investigation of three-dimensional boundary-layer separation are discussed in three parts. First, a number of variables are examined with emphasis on the qualitative determination of their relative importance with respect to the occurrence of separation. The significance of a variable was judged by its influence on the extent of separation, as indicated by the shadowgraphs and pressure distributions, as well as by its effect on the first occurrence of separation. Second, steadiness of the flow will be discussed. Third, data that will aid in the prediction of flare-induced boundary-layer separation are presented in terms of the significant variables.

RELATIVE IMPORTANCE OF VARIABLES

Of the variables considered, pressure rise is the basic quantity responsible for the occurrence of boundary-layer separation. The magnitude of pressure rise required to cause a specified extent of separation was influenced considerably by the adverse pressure gradient, the Mach number, and the Reynolds number based on boundary-layer thickness. The experimental variation of incipient-separation pressure rise with pressure gradient, Mach number, and Reynolds number might be caused by the variation in mixing between the outer stream and the dissipative flow near the wall. In the Crocco-Lees mixing theory (ref. 15), this momentum-transfer concept is the fundamental process which determines the pressure rise that can be supported by the flow. The theory shows that the rate of momentum transfer to the boundary layer is proportional to the rate of boundary-layer growth, and that momentum can be extracted from the boundary layer by an adverse pressure gradient (at a rate proportional to the pressure gradient) and by the viscous shear stress at the wall. It might be expected, therefore, that separation is less likely to occur for small pressure gradients than for large gradients. The rate of boundary-layer growth at any point on a cylinder is increased as Mach number is increased or as Reynolds number is decreased. This suggests that the pressure rise with no separation might also increase as Mach number is increased or as Reynolds number is decreased.

The ratio of cylinder diameter to boundary-layer thickness and the rate of heat transfer had a small influence on the separation characteristics. Unit Reynolds number, nose shape, cylinder length, and the method of promoting transition are variables that will be shown to be unimportant to the occurrence of boundary-layer separation in this investigation. A detailed discussion of each of these variables will be given.

Pressure rise.—The effect of over-all pressure rise on the growth of a separated region is illustrated in figure 5 by shadowgraphs of the bound-

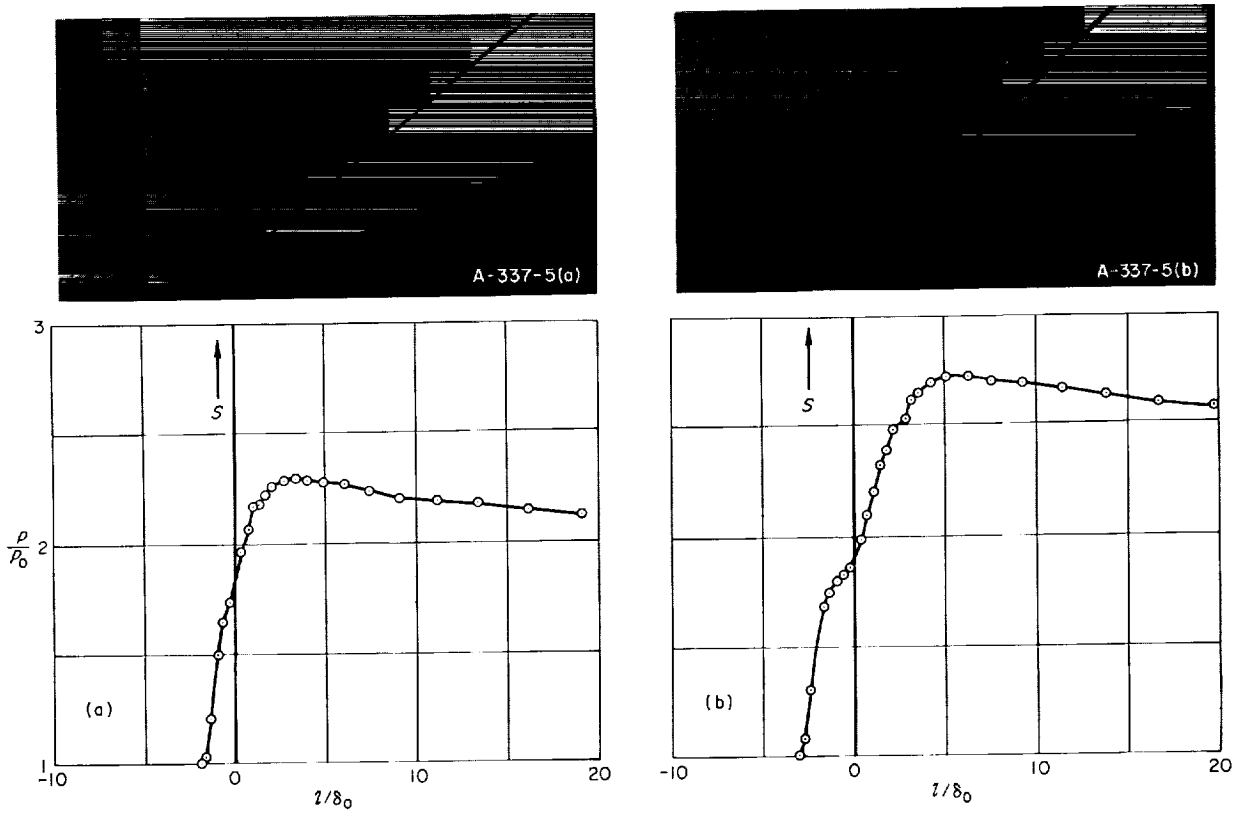

(a) CC20-a-1 (b) CC25-a 1

FIGURE 5.—Effect of over-all pressure rise on the flow separation ahead of a flare on a body of revolution; $M_\infty = 2.18$; $R_{\infty\delta_0} = 8.4 \times 10^4$.

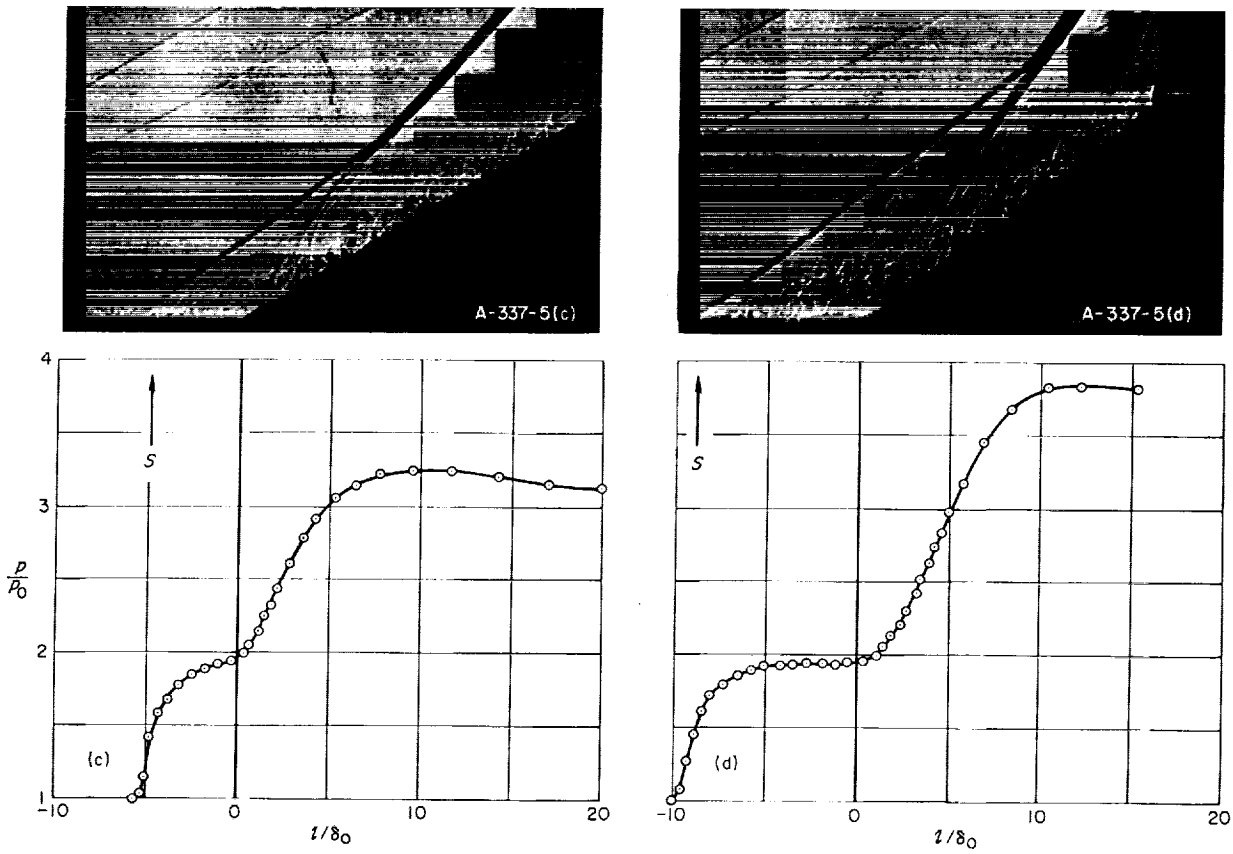

(c) CC30-a 1 (d) CC35-a-1

FIGURE 5.—Concluded.

ary-layer flow and the corresponding pressure distributions. The pressure rise was varied at constant Mach number, Reynolds number, and theoretical pressure gradient (theoretical pressure gradient is infinite) by varying the flow deflection angle of the compression corner. The pressure distributions are presented as the ratio of local static pressure to the static pressure on the model slightly upstream of the flare-induced pressure rise. The distance along the model is in terms of boundary-layer thickness. As the incipient-separation pressure rise was exceeded, the extent of separation increased rapidly.[1] This is evident from the shadowgraphs and from the increase in the size of hump in the pressure distributions. The extent of separation increased approximately $15\delta_0$ in length as the pressure rise was increased 65 percent.

Pressure gradient. Flare shape was varied to alter the adverse pressure gradient. The reduction in pressure gradient accomplished by curving the flare to a radius equal to $2.6D$ is illustrated in figure 6(a). The pressure distribution for the 25° compression corner is compared with three curved flares at the same test conditions. Boundary-layer separation is incipient on the 25° compression corner and the 45° curved surface; thus curving the flare surface increased the allowable deflection angle with no separation from 25° to 45°. The effect of pressure gradient on the extent of separation for a given deflection angle is shown in figure 6(b). Mach number, Reynolds number, over-all pressure rise, and the boundary layer approaching the adverse pressure gradient were identical for both flares. Pressure gradient is obviously an important variable, as shown by the completely attached boundary layer for the

[1] Length of separated region is difficult to determine accurately because of difficulty in establishing the reattachment point. An approximate measure of the size of separated region can be determined, however, from the distance between the separation point as indicated by the separation shock wave and the midpoint of the reattachment region as indicated by the reattachment shock waves.

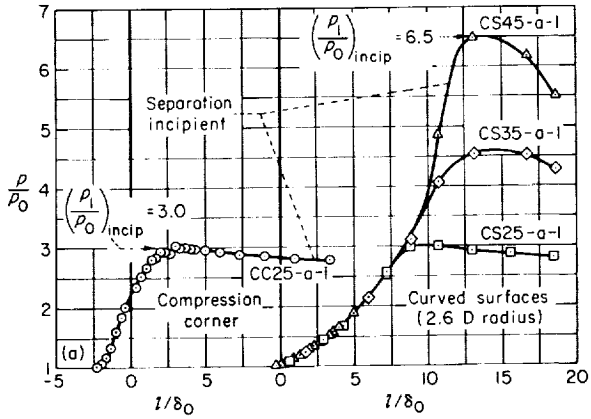

(a) Pressure gradients for the compression-corner and curved-surface flares; $M_\infty=2.3$; $R_{\infty\delta_0}=3\times10^4$.

FIGURE 6.—Comparison of compression-corner and curved-surface flares.

curved surface (reduced pressure gradient) in contrast with the large separated region and the very thick, turbulent layer downstream of reattachment for the compression corner (infinite theoretical pressure gradient).

Mach number.—The influence of Mach number on the extent of boundary-layer separation is presented in two ways. First, Reynolds number and pressure rise were held constant, then Reynolds number and model geometry were held constant. Reference 12 showed, for two-dimensional models, that Mach number variation in the higher Mach number and/or lower Reynolds number ranges had somewhat greater influence on the occurrence of separation than a Mach number variation in the lower Mach number and/or higher Reynolds number range. The magnitude of Mach number influence for the three-dimensional models could also be expected to vary. These data should, therefore, be accepted only as an example of the possible importance of Mach number.

Mach number influence with Reynolds number and pressure rise held constant is illustrated in figure 7. The flare angle was decreased from 35° to 25° as Mach number was increased to maintain a constant pressure rise. As Mach number

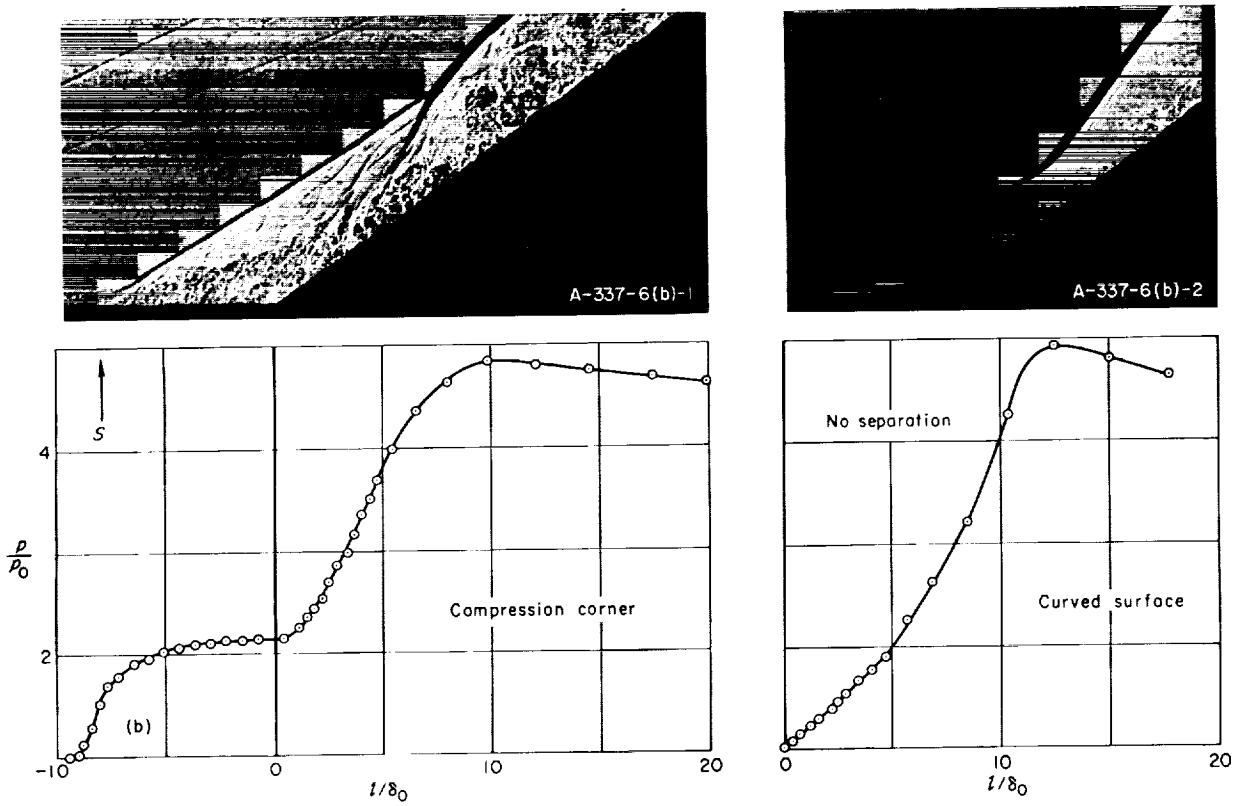

(b) Effect of flare shape on the extent of separated region; $\theta=35°$; $M_\infty=2.5$; $R_{\infty\delta_0}=1.1\times10^5$.

FIGURE 6.—Concluded.

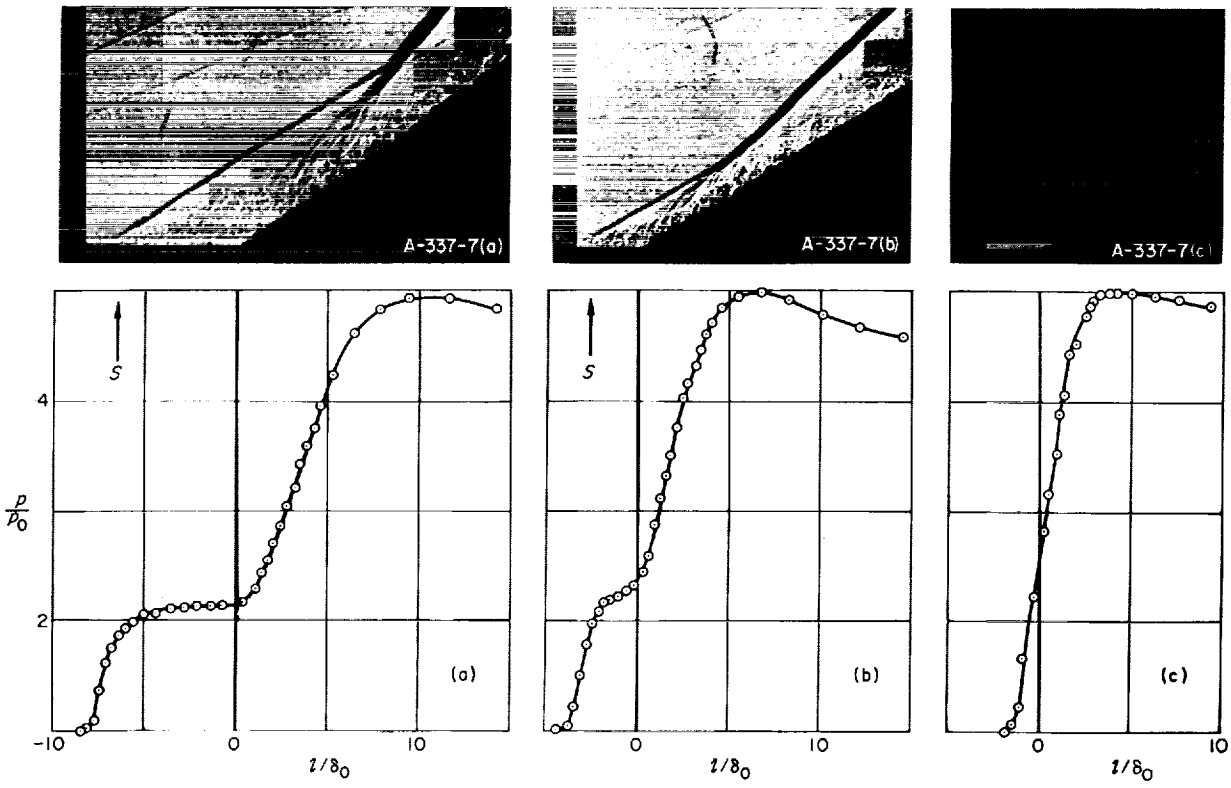

(a) $M_\infty = 2.56$ (b) $M_\infty = 2.95$ (c) $M_\infty = 3.52$

FIGURE 7. Effect of Mach number on the flow separation ahead of a flare on a body of revolution; pressure rise and Reynolds number constant; $p_1/p_0 = 5$; $R_{\infty\delta_0} = 9.7 \times 10^4$.

was increased the size of separated region decreased considerably, as is witnessed by the downstream movement of the separation point in the shadowgraphs, and the decreased longitudinal extent of the hump in the pressure distribution.

Mach number influence with Reynolds number and model geometry held constant is illustrated in figure 8. It is of more practical interest to consider constant flare angle rather than constant pressure rise since geometry generally will be constant during actual flight. The true influence of Mach number is not observed, however, because pressure rise increased as Mach number increased. This compensating effect (see section on influence of pressure rise) resulted in a lesser change in the extent of separation for a given Mach number change than for the condition of constant pressure rise. Mach number is, however, a very important variable affecting boundary-layer separation phenomena in either case.

Reynolds number.—The Reynolds number used in boundary-layer flow studies should be based upon some boundary-layer dimension, especially when transition is artificially induced or when transition location is not constant. In the present investigation, δ_0 was used as the reference dimension and unit Reynolds number (i.e., R_∞/inch) was varied to change boundary-layer Reynolds number. The possible influence of unit Reynolds number on boundary-layer separation was determined by comparing the separation characteristics of two geometrically similar models (Models CC30-a-2 and CC30-a-2-1, fig. 1). The unit Reynolds number for the small body was approximately 2.5 times that for the large body for constant values of R_{δ_0} and D/δ_0. (The possible significance of this ratio will be discussed in a following section.) The comparison of separation characteristics is shown in figure 9 in terms of the Mach number at which separation was incipient on the two models for a range of boundary-layer Reynolds numbers. At all the test conditions represented, no measurable influence of unit Reynolds number is indicated.

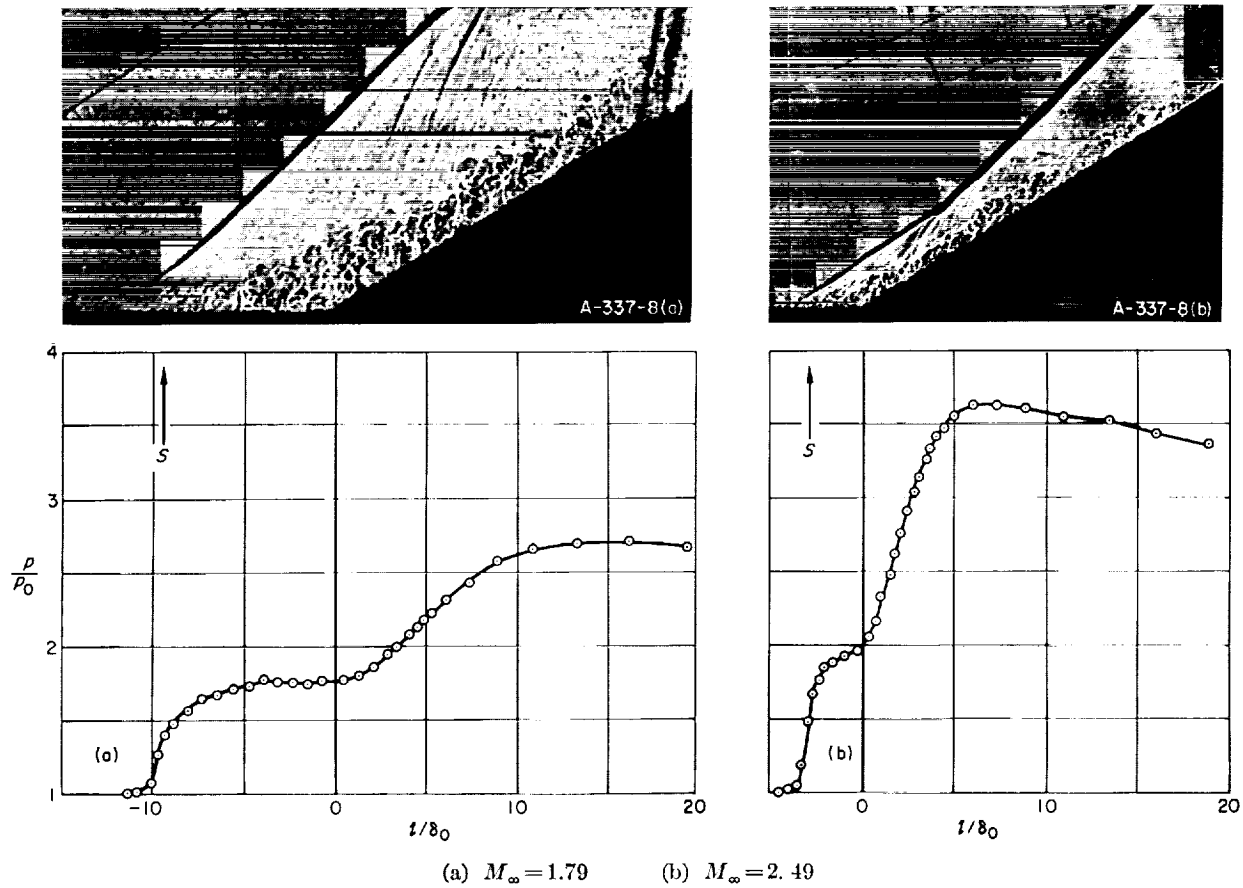

(a) $M_\infty = 1.79$ (b) $M_\infty = 2.49$

FIGURE 8.—Effect of Mach number on the flow separation ahead of a flare on a body of revolution; flare angle and Reynolds number constant; CC30-a-1; $R_{\infty \delta_0} = 8.3 \times 10^4$.

This variable need not be considered, therefore, in subsequent data presentations.

Boundary-layer Reynolds number is shown in figure 10 to have a measurable influence on the size of separated region at the compression-corner flare. This influence was, however, generally not so important as the influence of Mach number variation. As will be shown later, the effect of Reynolds number was larger in the higher Mach number and/or lower Reynolds number ranges.

Method of promoting transition.—The method of promoting transition could affect the occurrence of separation through its influence on boundary-layer characteristics, such as thickness, profile, and effective boundary-layer Reynolds number. In this investigation boundary-layer trips were used on most models to ensure a turbulent boundary layer. The possible importance of this variable will, therefore, be examined for several methods of promoting transition by comparison of the incipient-separation conditions on a typical model geometry.

Incipient-separation data obtained using three types of boundary-layer trip are compared with data for the condition of natural transition in figure 11. The three trips employed were a wire ring located on the cylinder, distributed roughness over the entire nose, and a base-type trip located at the nose-cylinder juncture. No measurable difference was detected in the Mach number for incipient separation. Further, the velocity profile parameters for the boundary layers on the various models showed no consistent differences

Ratio of cylinder diameter to boundary-layer thickness.—The ratio D/δ_0 is a measure of the degree of three-dimensionality of a boundary layer on a cylinder. For a very large ratio the pressure rise in the region of the corner should approach a two-dimensional value, whereas the pressure rise for a very small ratio should approach that for a

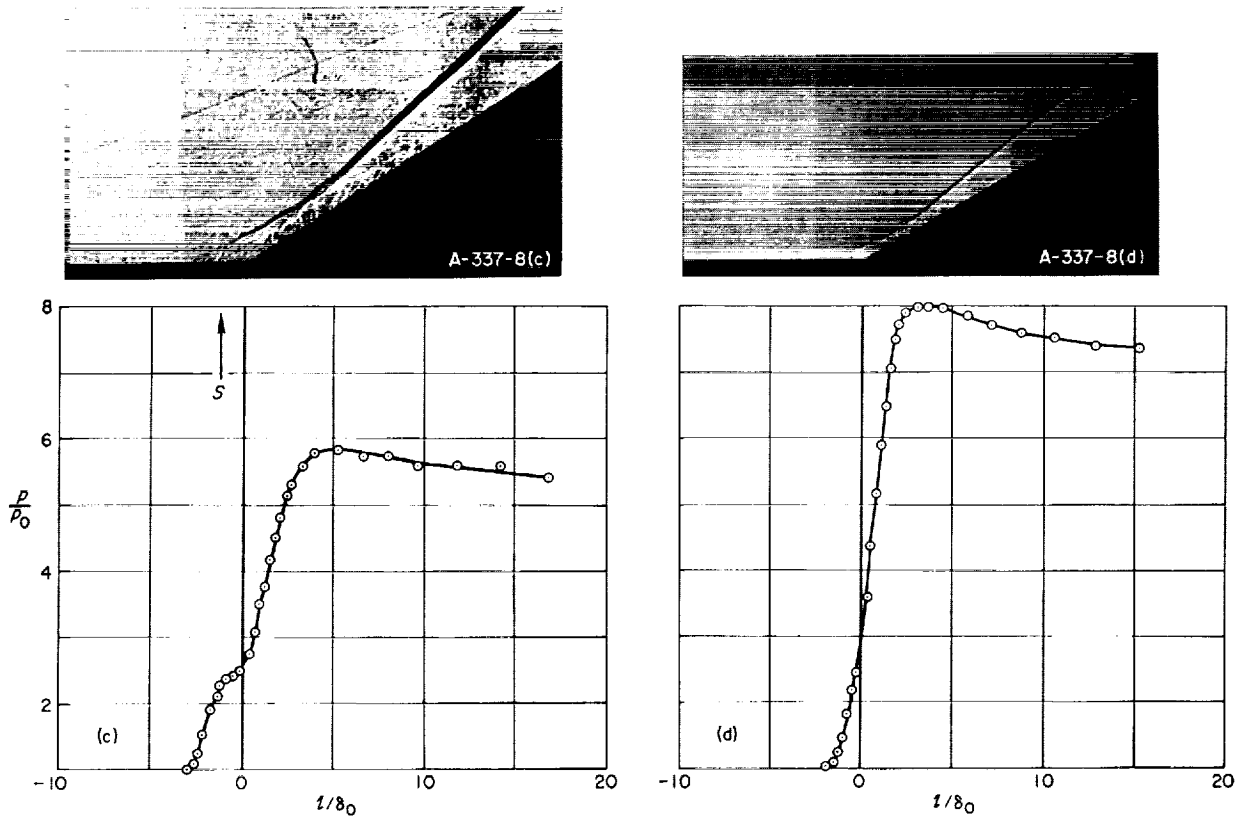

(c) $M_\infty = 3.31$ (d) $M_\infty = 4.07$

FIGURE 8.—Concluded.

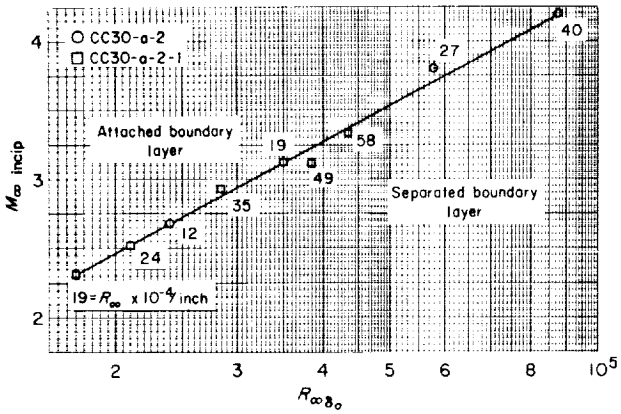

FIGURE 9.—Incipient separation independent of free-stream Reynolds number; $\theta = 30°$.

cone. Although not shown here, the experimental values of maximum pressure rise near the corner indicate this trend. It was expected, therefore, that separation would occur sooner on a configuration with large D/δ_0 (larger maximum pressure rise) than for small D/δ_0 (smaller maximum pressure rise).

Two sets of data were available for evaluating the influence of this ratio. First, the data of figure 11 obtained with models of constant cylinder diameter but with different boundary-layer trips represent a variation in D/δ_0 by a factor of 2 (the most severe trip, distributed roughness, thickened the boundary layer the most) which was not sufficient to produce a detectable change in incipient-separation Mach number. Second, the data shown in figure 12 were obtained specifically to evaluate the influence of D/δ_0. A small diameter cylinder with a thickened boundary layer was compared with a larger diameter cylinder with a thinner boundary layer. Included also are two-dimensional data from reference 12. The figure shows the expected decrease in incipient-separation Mach number corresponding to a decrease in D/δ_0. In all subsequent data presentations, D/δ_0 varies less than a factor of 2 and thus need not be considered further in this investigation.

Nose geometry.—Nose geometry could influence flare-induced boundary-layer separation indirectly

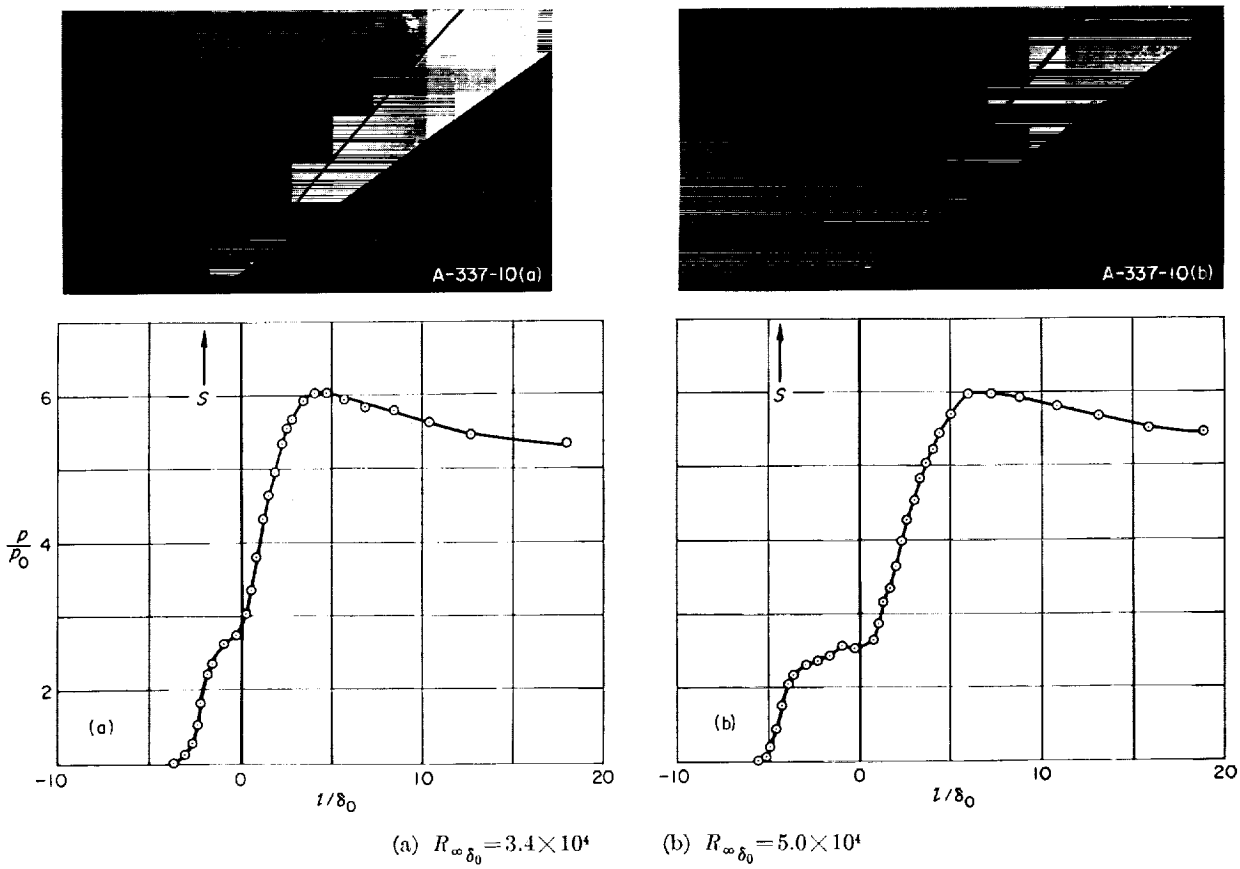

(a) $R_{\infty\delta_0}=3.4\times10^4$ (b) $R_{\infty\delta_0}=5.0\times10^4$

FIGURE 10.—Effect of boundary-layer Reynolds number on the flow separation ahead of a flare on a body of revolution; $M_\infty=2.92$; CC35-a 1.

by altering variables that are known to be important to the separation phenomena, such as Mach number and Reynolds number at the boundary-layer edge, boundary-layer thickness and profile, and the pressure gradient on the cylinder. A sharp, conical nose was assumed to have the least influence on the flow over the cylinder and was, therefore, used on most models. The requirement that the nose shape be an unimportant variable was deemed necessary for a valid basis of comparison of flow separation for two-dimensional and three-dimensional compression corners. The possible influence of nose geometry was investigated to extend the usefulness of the results of this investigation to configurations employing blunter nose shapes.

Before the conditions for incipient separation are compared for blunt and sharp models, it is necessary to determine whether the turbulent boundary layers on the blunt models were fully developed. This question arose because the boundary layer on a blunt-nosed model was enveloped by a layer of air at a Mach number and Reynolds number much lower than free-stream values. Consequently, the Mach number and Reynolds number at the boundary-layer edge are less than for a sharp-nosed model. This layer of low Reynolds number air favors a laminar boundary layer and makes it difficult to produce a turbulent boundary layer. Whether or not the boundary layers are fully developed will be discussed in the following paragraphs. An additional question that arises with respect to the blunt models is whether the conditions at the boundary-layer edge or in the free stream should be used to define the separation phenomena. Since the answer is not obvious, both edge and free-stream values will be examined for the purpose of determining the basis for comparing the boundary layer in a shear layer on a blunt body with the boundary layer on a sharp-nosed body.

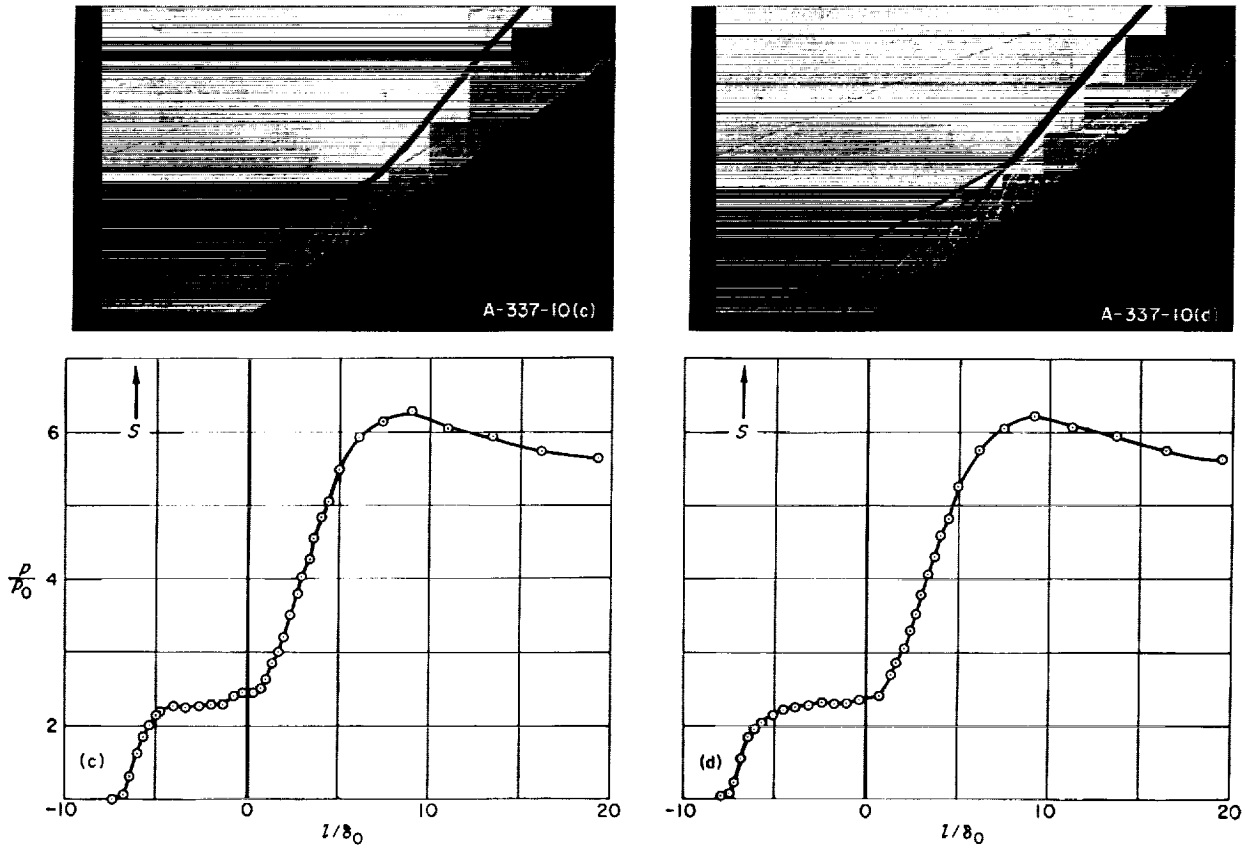

(c) $R_{\infty \delta_0} = 8.3 \times 10^4$ (d) $R_{\infty \delta_0} = 11.1 \times 10^4$

FIGURE 10.—Concluded.

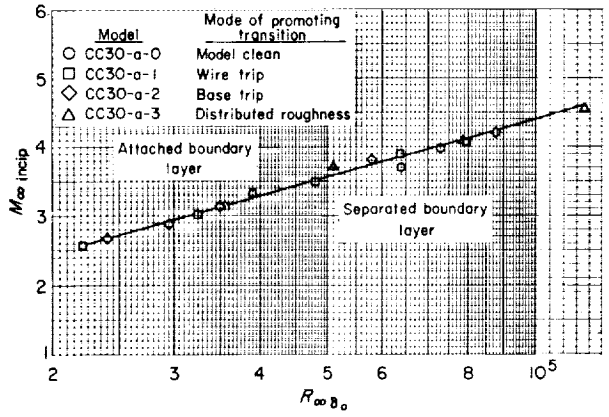

FIGURE 11.—Effect of the mode of promoting transition on the Mach number for incipient separation for a 30° compression corner.

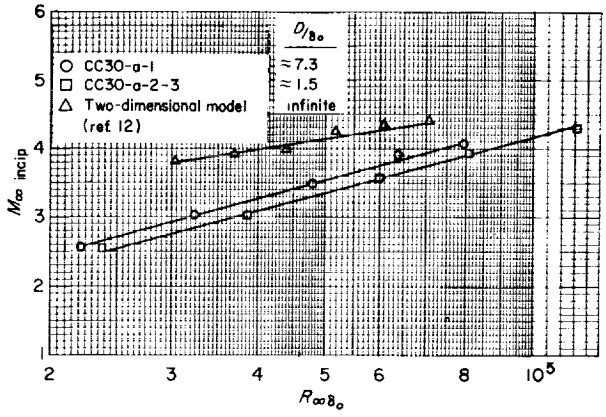

FIGURE 12.—Effect of D/δ_0 on the Mach number for incipient separation for a 30° compression corner.

The velocity-profile parameter is a measure of the degree to which the turbulent boundary layer is developed. This parameter could not be obtained for all data of this investigation because surveys did not always extend far enough into the boundary layer. (The prime purpose of the surveys was to determine δ_0; thus complete profiles were not always taken.) Where complete profiles

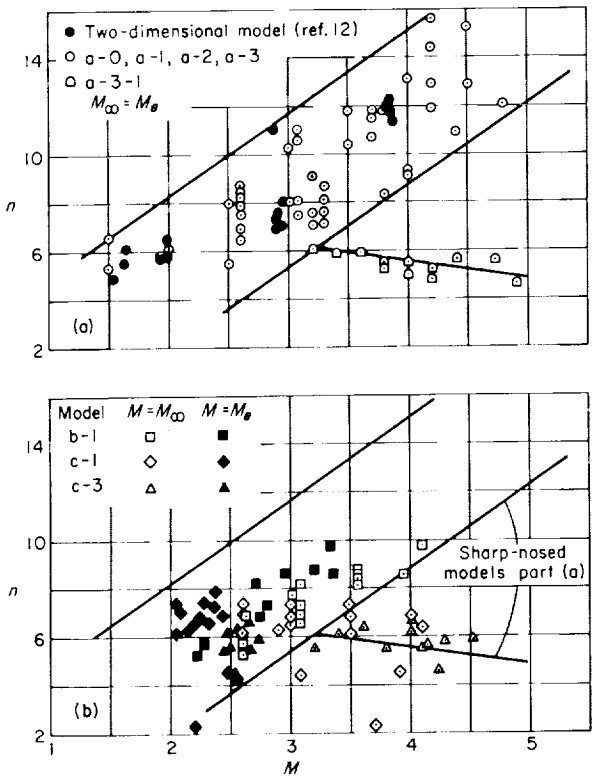

(a) Sharp-nosed models.

(b) Blunt-nosed models.

FIGURE 13.—Velocity-profile parameter.

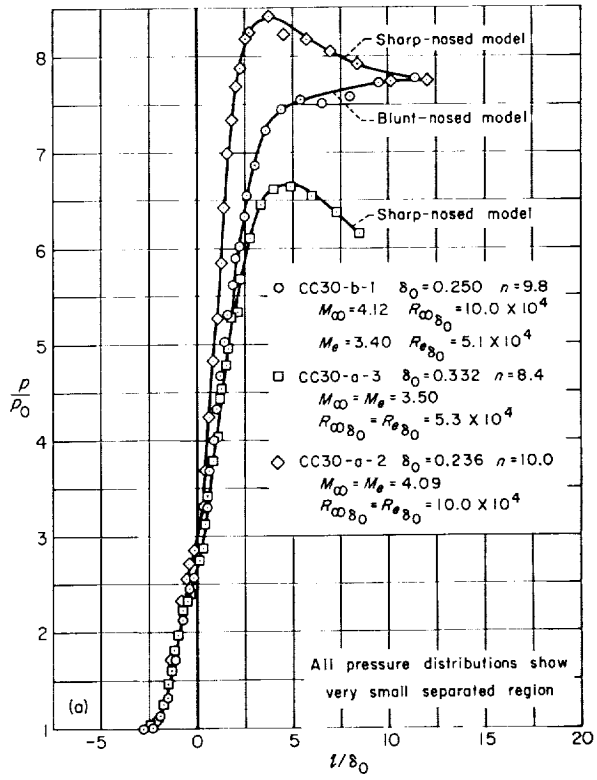

(a) Boundary layer fully developed on all models.

FIGURE 14.—Comparison of pressure distributions on blunt-nosed and sharp-nosed cylinder-flare configurations.

were obtained, however, the values of n were computed and are presented in figure 13. This figure was used to determine whether the turbulent boundary layers on the blunt models and the short models were fully developed. The profile parameters shown represent a range of Reynolds numbers but were plotted only as a function of Mach number. The data for the blunt-nosed models were plotted as a function of M_e as well as M_∞ ($M_e=M_\infty$ for the sharp-nosed models). The long model with a sharp nose and a severe boundary-layer trip, tested at high Reynolds numbers, would be the one most likely to have a fully developed turbulent boundary layer. Since there was no consistent difference in the value of n for the long models with sharp noses for all trips and test conditions, it was assumed that the values of n for these models represented fully developed boundary layers (see fig. 13(a), models a-0, a–1, a–2, a–3). The two-dimensional model of reference 12 also had a fully developed boundary layer. This model had a very severe boundary-layer trip. Data which deviated from the approximate region represented by the circles in figure 13(a) were assumed to be not fully developed, for example, model a–3–1. For the case of the blunted 45° conical-nosed model (b–1), the boundary-layer profiles are indicated to have been fully developed regardless of whether M_e or M_∞ was used in plotting the values of n. This is not true for the models with hemispherical noses (c–1 and c–3). For these models the boundary-layer profiles are indicated as having been fully developed when n is plotted as a function of M_e, but not when plotted as a function of M_∞. The results for the hemispherical-nosed models, therefore, are inconclusive.

Pressure distributions on a cylinder-flare configuration were also examined in an attempt to gain further information as to whether the turbulent boundary layers on the hemispherical-nosed model were fully developed. In figure 14(a) the pressure distribution on a model with a blunted conical nose is compared with the pressure distributions on two sharp-nosed models, all with

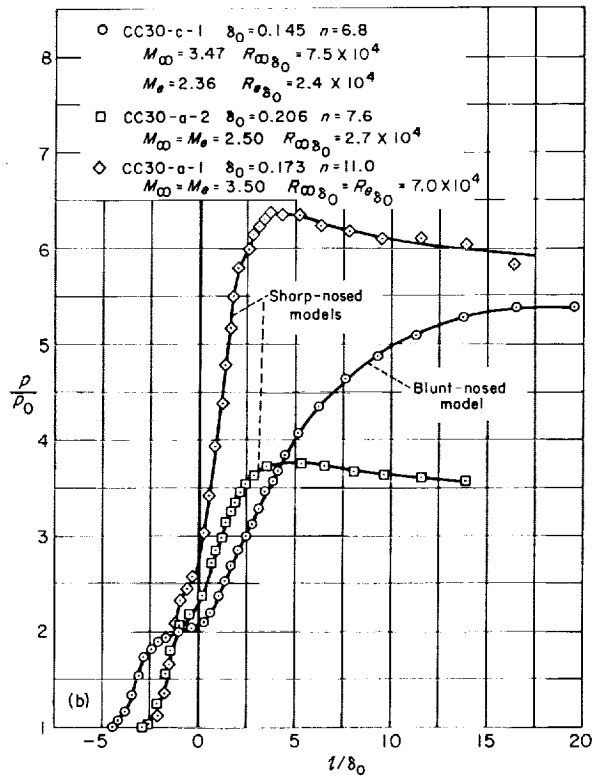

(b) Boundary layer not fully developed on the blunt-nosed model.

FIGURE 14.—Concluded.

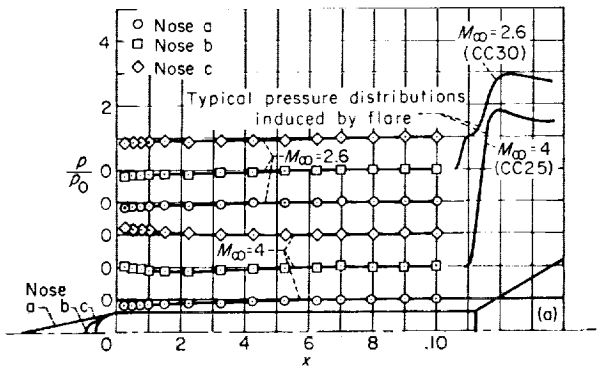

(a) Pressure distribution.

FIGURE 15.—Influence of nose shape on the flow over a cylinder-flare model.

30° flares. The data for one of the sharp-nosed models correspond to the free-stream conditions of the blunt model; the data for the second sharp-nosed model correspond to the boundary-layer-edge conditions of the blunt model. The velocity-profile parameters, as a function of Mach number, were all of the magnitude that would be expected for fully developed boundary-layer profiles. The extent of separation, as indicated by the pressure distribution, was essentially identical for the three conditions. This indicates that the boundary layers were similar. In the region of the corner, the pressure distribution correlates better on the basis of boundary-layer-edge conditions, whereas the final pressure attained on the flare correlated better on the basis of free-stream conditions. This observation was also noted in other such comparisons. Figure 14(b) compares, in the same manner as that used in figure 14(a), a pressure distribution for a hemispherical-nosed model with pressure distributions for two sharp-nosed models. The comparison of pressure distributions shows that the hemispherical-nosed model had a larger separated region, thus indicating that the boundary layer for this model was not fully developed. This was the condition indicated by the correlation of the boundary-layer profile parameter n with free-stream Mach number (fig. 13(b)) whereas the correlation of n with edge Mach number indicated a fully developed layer. The reason for the apparent correlation of n as a function of edge Mach number is not known, but it appears this correlation was accidental and is misleading in view of the discussion just presented. A further indication that the boundary layers on the hemispherical-nosed models were not fully developed is provided by subsequent comparisons of incipient separation conditions for the various models.

The influence of nose shape on the surface pressure distribution along the cylinder is indicated by figure 15(a) which presents typical static-pressure distributions on the cylinder for the three nose geometries. For the range of Mach numbers of this investigation the nose-induced pressure gradients were negligible compared to typical flare-induced pressure gradients. At higher Mach numbers induced pressure gradients for blunt noses are sizable. The gradients are favorable, however, so the tendency toward separation of a fully developed turbulent boundary layer at the flare might be reduced.

The Mach number at which flare-induced separation was incipient for two nose shapes is shown in figure 15(b) for the models with a cylinder length of $9D$. The hemispherical-nosed model was excluded from this comparison because

the boundary layer on this model did not have a fully developed velocity profile. (See preceding discussion for figs. 13 and 14.) Figure 15(c) compares incipient separation conditions on the models with cylinder length of $4.2D$. None of these short models had fully developed boundary-layer profiles, but, as figure 13 shows, the values of n for these models were nearly the same; thus this comparison was considered valid. Figures 15(b) and 15(c) show that the data for the blunt models correlate with the data for the sharp models up to $M_\infty = 4.5$ regardless of whether conditions were based on free-stream values or boundary-layer-edge values. Nose shape had no influence on the occurrence of boundary-layer separation.

The influence of nose shape on the flow in the region of the flare will now be examined qualitatively in terms of the unit Reynolds number and Mach number of the free stream. This examination was considered worth while because the boundary-layer thickness and, therefore, R_{δ_0} are more difficult to determine for a configuration with a blunt nose than for one with a sharp nose. The possibility is therefore examined of using data for a sharp-nosed configuration to obtain a first approximation for the occurrence of separation on a blunt-nosed configuration. In this examination boundary-layer thickness was of no concern, but the existence of a fully developed turbulent layer was essential. Figure 15(d) shows the flow in the region of a 30° flare for two models, identical except for nose shape, tested in identical streams. The obvious effects of blunting the nose were to extend the upstream influence of the flare, to decrease the pressure gradient a sizable amount, and to decrease the maximum pressure rise. At high Mach numbers the flow for the blunt model will become increasingly different from that for a sharp-nosed model because the ratio of Mach number within the shear layer to the free-stream Mach number becomes less. It appears, however, that for low Mach numbers and/or small amounts of bluntness, the conditions for the first occurrence of separation on blunt bodies can be approximated if the bluntness is disregarded and data for sharp-nosed models are used to predict the occurrence of separation without regard to shear layers or to how the boundary-layer thickness and profile are affected by the blunt nose.

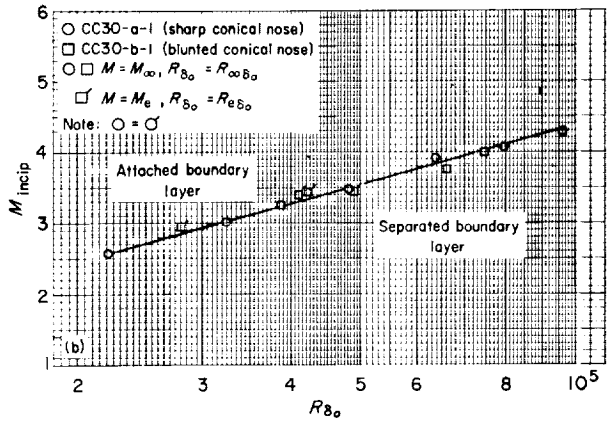

(b) Incipient-separation conditions for the compression corner with $(L/D)_{cyl} = 9.0$; boundary layers fully developed.

FIGURE 15.—Continued.

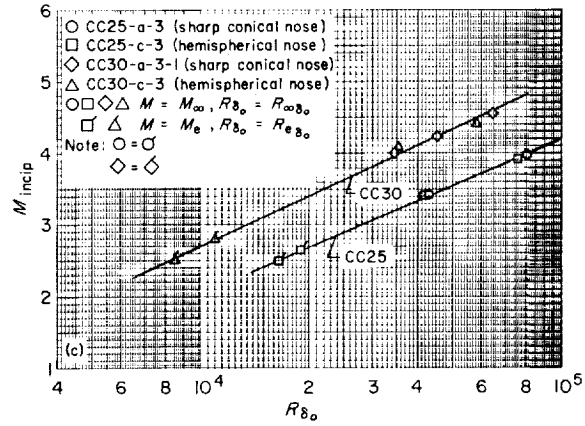

(c) Incipient-separation conditions for the compression corner with $(L/D)_{cyl} = 4.2$; boundary layers were not fully developed, but were similar.

FIGURE 15.—Continued.

Cylinder length.—The separation phenomena at a flare should not be influenced by the cylinder length if the flare is beyond the pressure field induced by the nose, if changes in δ_0 are accounted for through the quantities D/δ_0 and R_{δ_0}, and if the turbulent boundary layer attains a fully developed profile. The very small pressure gradients induced by the nose (fig. 15(a)), therefore, suggest the possibility that the cylinder length could be reduced from the principal length ($9D$) used in this investigation with no influence on the separation phenomena. Incipient conditions were compared for models with cylinder lengths of $4.2D$ and $9D$.

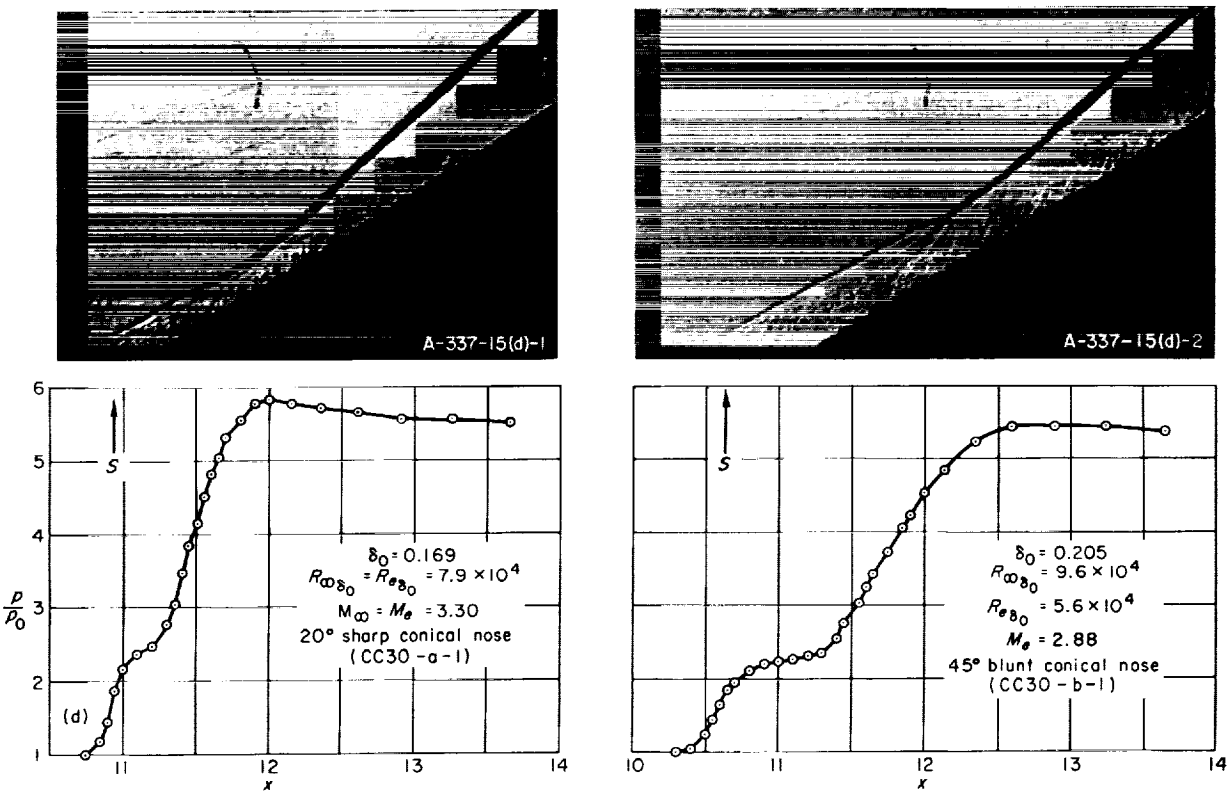

(d) Flow in the region of a flare for identical free-stream conditions; $M_\infty = 3.30$; R_∞/inch $= 47 \times 10^4$; $(L/D)_{cyl} = 9.0$.

FIGURE 15.—Concluded.

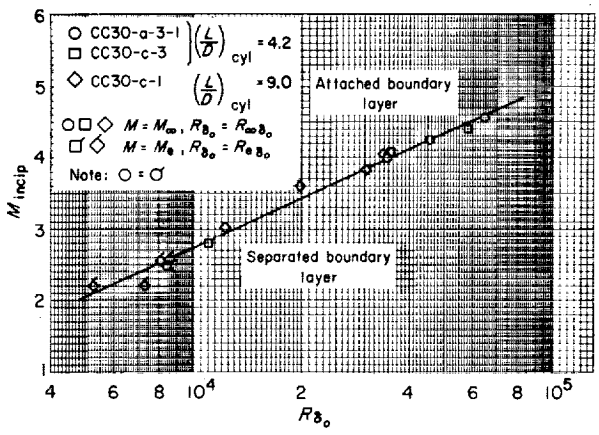

FIGURE 16. Influence of cylinder length on the occurrence of separation. Boundary layers were not fully developed, but were similar (see fig. 13).

The influence of cylinder length on the Mach number at which boundary-layer separation was incipient for a cylinder-flare configuration is shown in figure 16. The turbulent boundary layers on the models considered in figure 16 did not have fully developed profiles, but figure 13(b) indicates that the boundary layers were similar (by virtue of similar values of n). Figure 16 shows cylinder length had no influence on the occurrence of separation at the flare. This conclusion for the case of the not fully developed turbulent boundary layer would also be expected to apply in the fully developed case in view of the preceding discussion of the behavior of the two boundary-layer cases (figs. 14 and 15).

Velocity-profile parameter.—The data presented in figures 14 to 16 indicate that the actual magnitude of n is not important to the separation phenomena if its value is in the range that represents a fully developed boundary layer. On the other hand a boundary layer with a velocity profile that was not fully developed was shown to have an increased tendency toward separation. Figure 17(a) shows the influence, on the incipient-separation Mach number, of boundary layers which do not have fully developed profiles. These data support the observation made previously

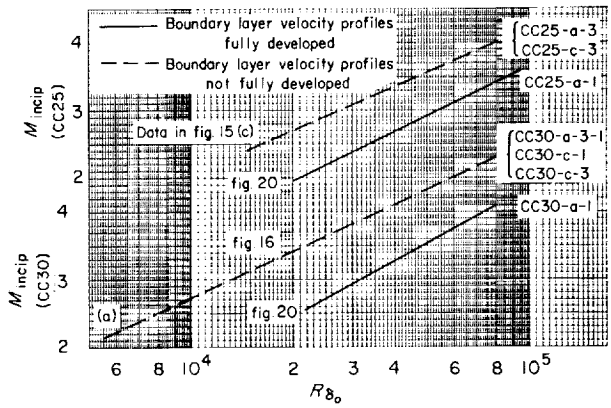

(a) Mach number for incipient separation.

FIGURE 17.—Comparison of the separation characteristics of turbulent boundary layers which are fully developed with those which are not fully developed.

that a turbulent boundary layer which is not fully developed will be more prone to separation than a fully developed layer.

Figure 17(b) shows a comparison of the flow in the region of a 30° flare for a boundary layer with a fully developed profile and for one that was not fully developed. The test conditions were chosen so that separation was incipient for the fully developed layer, and, therefore, a small region of separated flow existed for the layer not fully developed (see fig. 17(a)). In spite of the fairly large effect on incipient conditions shown in figure 17(a), the pressure distribution and length of separated region were not greatly different. For the boundary layer which was not fully developed, the upstream influence of the flare was slightly greater (approximately $1.5\delta_0$), and the maximum pressure rise and pressure gradient were slightly less than for the fully developed boundary layer. The incipient-separation data for the models with fully developed boundary layers can, therefore, be used to give a first approximation of the flight conditions for

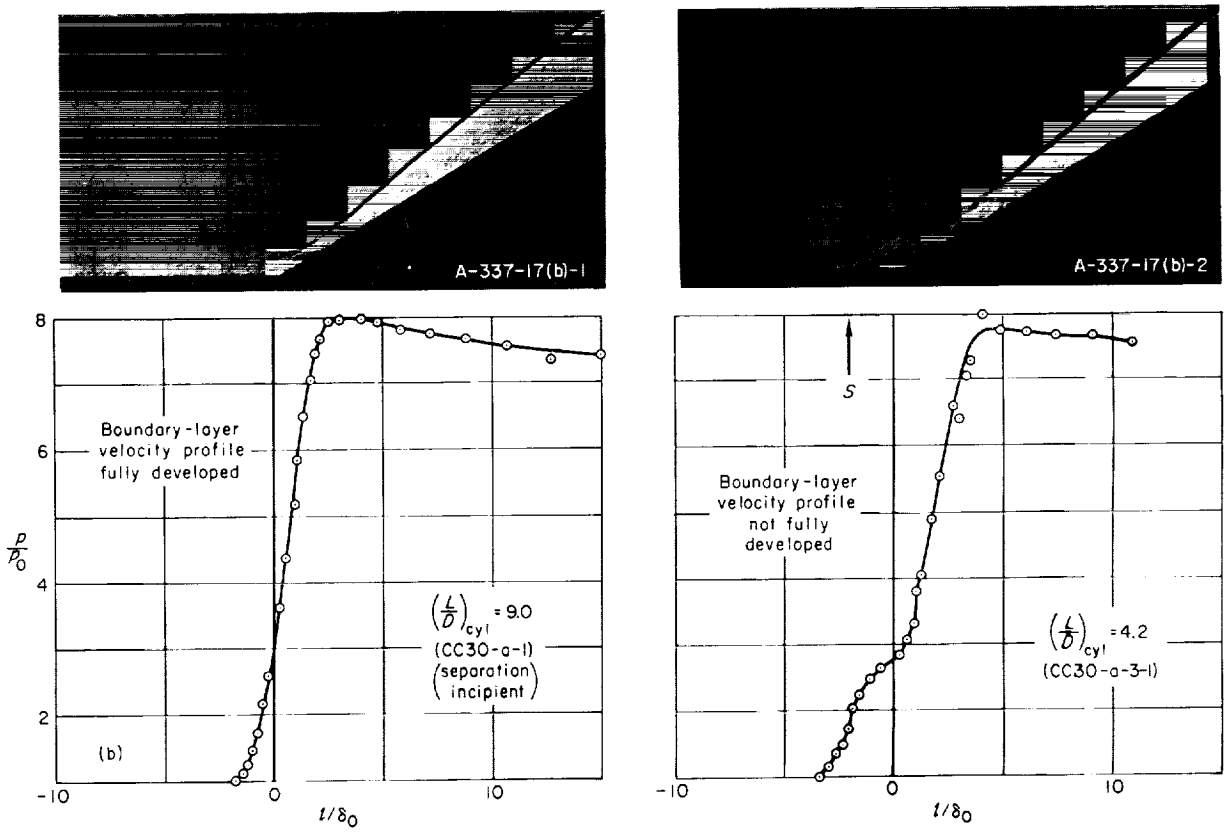

(b) Flow in the region of the flare; $M_\infty = 4.1$; $R_{\infty_{\delta_0}} = 8.0 \times 10^4$.

FIGURE 17.—Concluded.

the occurrence of separation of a turbulent boundary layer which does not have a fully developed profile. This estimation will, however, predict no separation when there is actually a small separated region.

Heat transfer.—The qualitative influence of heat flow into the model was obtained using the solid copper model cooled with liquid nitrogen. Typical results are shown in figure 18 for one particular Mach number and Reynolds number. The separation point moved downstream about $0.2D$ or 1δ, based on a rough estimate of boundary-layer thickness. Heat transfer showed the same qualitative influence on the size of separated region for other Mach numbers and Reynolds numbers. The pressure-distribution data of reference 16 also show a small decrease in the extent of separated region for heat flow into a two-dimensional model. It is indicated, then, that data on incipient separation obtained with zero heat transfer will, therefore, give a slightly conservative estimate of the first occurrence of separation when applied to configurations with heat flow into the surface.

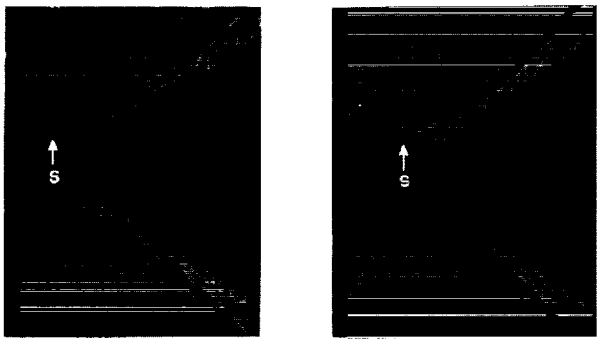

(a) Wall temperature = 56° F
Adiabatic wall temperature = 56° F

(b) Wall temperature = −276° F
Adiabatic wall temperature = 56° F

FIGURE 18. Qualitative influence of heat transfer on the extent of boundary-layer separation; CC35-a-2; $M_\infty = 3.1$; $R_\infty = 64 \times 10^4$/inch.

FLOW STEADINESS AND HYSTERESIS EFFECTS

Compression corners.—Turbulent attached flow for the compression-corner flare was observed to be steady.[2] Small separated regions (i.e., less than about $5\delta_0$ in length) appeared to be as steady as the completely attached flows. The flow became unsteady for larger separated regions, and the unsteadiness increased as the size of separated region increased. When test conditions were changed in the direction that promoted separation at the compression-corner flare, a region of separated flow appeared and grew gradually as the incipient conditions were exceeded. As the test conditions were reversed, the region of separation decreased gradually and disappeared. No apparent hysteresis was detected in the conditions for the appearance and disappearance of separation.

Curved surfaces.—Turbulent attached flow on the curved-surface flare, as on the compression-corner flare, was always steady but when separation occurred at the curved-surface flare the flow was always extremely unsteady. This unsteadiness was evidenced by the random shock pattern that emanated from the turbulence within the separated region (see photographs in figs. 19(b) and 19(c)). Although not shown here, successive photographs taken at a single test condition showed this shock pattern to change with time. The separation point also oscillated over a distance of several boundary-layer thicknesses. This change with time of the location of the separation point was responsible for the discontinuity in the separation shock shown in figure 19, which resulted from the necessity of recording the flow pattern on two different photographs taken a short time apart.

Separated regions appeared (and disappeared) very abruptly on the curved-surface flares. An example of these abrupt changes in flow pattern is illustrated in figure 19 for the 45° flow-deflection angle. The separation on these flares was characterized by a sudden change from a completely attached, steady flow to a large, unsteady, separated region (figs. 19(a) and 19(b)) and vice versa (figs. 19(c) and 19(d)). The very large change in pressure distribution occurred as the boundary layer separated because the effective flow-deflection angle was considerably less than the geometric angle of the flare for the large regions of separation.

A hysteresis in the appearance and disappearance of the separated region often occurred for the curved-surface flares. The data shown in figure 19 for a 45° flare illustrate this hysteresis.

[2] In reference 1 it was shown that whenever unsteadiness was detected in high-speed motion pictures it could also always be detected when viewed on the shadowgraph screen, or by examination of spark shadowgraphs. Shadowgraphs of steady and unsteady flow are shown in reference 12. The shadowgraph was, therefore, used in this investigation to assess qualitatively the steadiness of the flow.

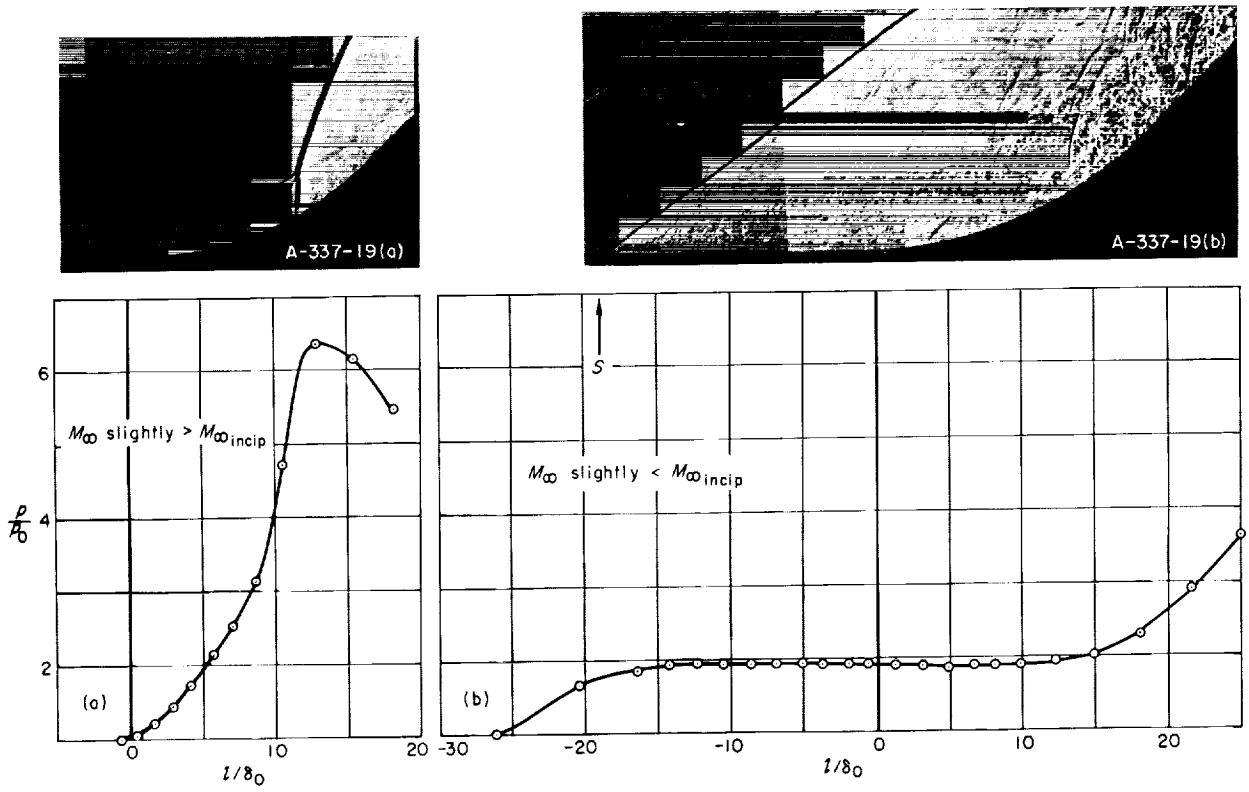

(a) $M_\infty = 2.33$; M_∞ decreasing. (b) $M_\infty = 2.15$; M_∞ decreasing.

FIGURE 19. Illustration of the occurrence of separation as observed on the curved-surface flares; CS45-a-1; $R_{\infty\delta_0} \approx 6 \times 10^4$.

The Mach number at which separation appeared was always lower than the Mach number at which separation disappeared. The amount of hysteresis was dependent on Reynolds number. At the lowest Reynolds number it was nearly zero; at the highest it was as shown in figure 19. A range of Mach numbers resulted for which the flow could be either attached or separated, depending upon whether the flow was initially attached or initially separated before entering this Mach number range. Above this Mach number range the flow was always attached; below it was always separated. Very little hysteresis was observed for the 35° flare and separated flow did not occur on the 25° flare; thus the sizable hysteresis illustrated in figure 19 appears to have been confined to the largest flow-deflection angles and the highest Reynolds numbers.

PREDICTION OF FLARE-INDUCED BOUNDARY-LAYER SEPARATION

Data presented in figures 20 to 23 will serve as a guide to predict whether or not separation is probable at a flare on a body of revolution. These data were obtained for artificially tripped boundary layers on sharp-nosed models with relatively long cylindrical forebodies; however, it has been shown previously that these data should also apply to cylinder-flare models with blunt noses, shorter cylindrical forebodies, and other modes of promoting transition, including natural transition. The turbulent boundary layer must, however, have a fully developed velocity profile. These data for configurations at temperature equilibrium give a slightly conservative estimate of the first occurrence of separation on a configuration with heat flow into the surface. The data are presented as curves for incipient separation (i.e., curves which divide the test conditions for which separation can be expected from the test conditions for which the boundary layer will be attached). Pressure rise and/or flow-deflection angle required for the first occurrence of separation will be presented as a function of Reynolds number based upon boundary-layer thickness, Mach number, and model shape.

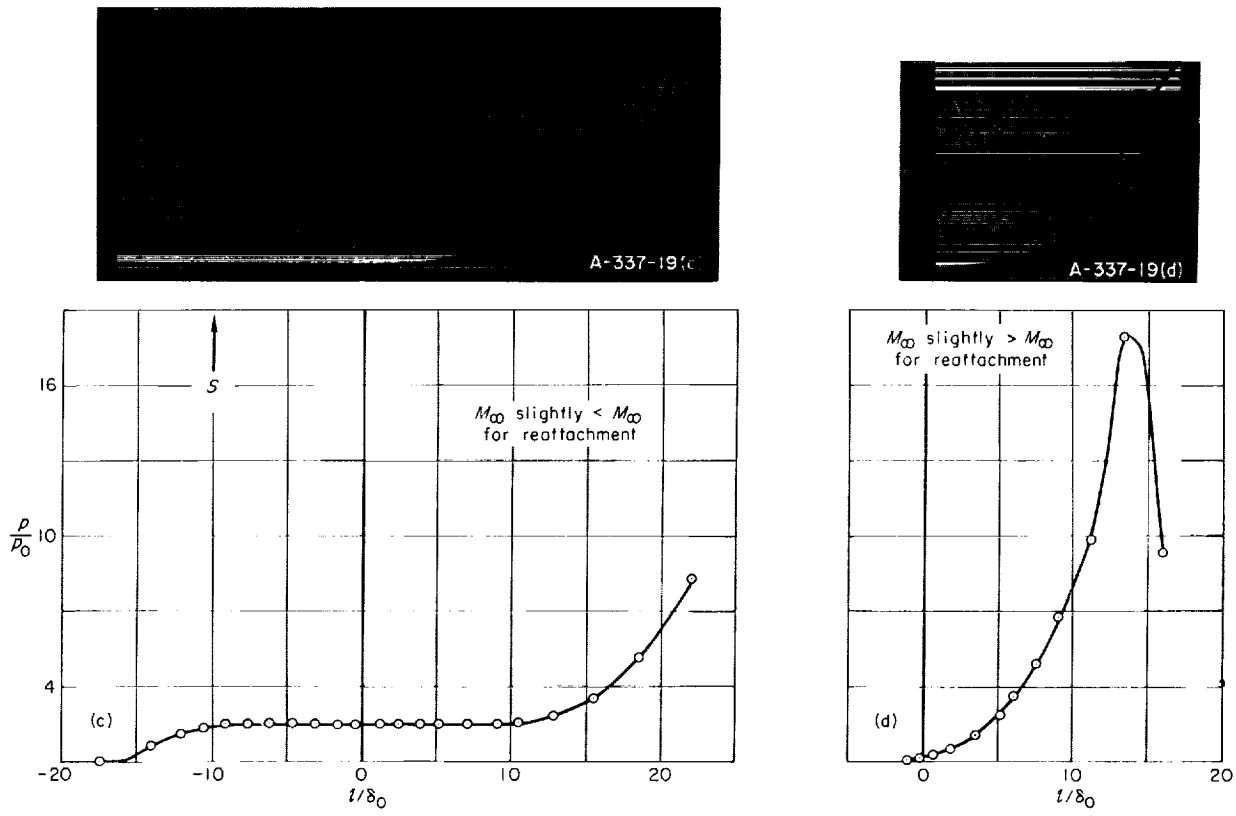

(c) $M_\infty = 3.22$, M_∞ increasing. (d) $M_\infty = 3.47$; M_∞ increasing.

FIGURE 19.—Concluded.

Compression-corner flares. The basic data for the compression-corner flares are shown in figure 20 in terms of the Mach number at which flare-induced separation is incipient as a function of the Reynolds number based on boundary-layer thickness. Each curve represents the dividing line between the test conditions for which the boundary layer was always attached at the flare (above the curve) and the test conditions for which there was always separation at the flare (below the curve). Also indicated on the figure is the approximate minimum Reynolds number (or maximum Mach number) for which there was a fully developed turbulent boundary layer at the flare. This specific limit curve applies only to these data because of the large number of factors which normally affect transition Reynolds number. Such a limit has general importance, however, in that it indicates the existence of a very definite limit to the extent to which Mach number may be increased (or Reynolds number decreased) to avoid separation. Obviously the incipient-separation curves cannot be projected beyond such limits because the laminar or transitional boundary layer which would then exist would separate from the surface more readily than a turbulent boundary layer.

The influence of Mach number on the pressure rise necessary for incipient separation has been obtained by cross-plotting the data of figure 20. The resulting curves shown in figure 21 define the maximum pressure rise possible with no separation as a function of Mach number and Reynolds number. The curves divide the test conditions for which the boundary layer was always attached at the flare (below the curve) from those for which the boundary layer was always separated at the flare (above the curve). The maximum incipient-separation pressure rise possible for compression corners is also shown in figure 21. This limit, explained in conjunction with figure 20, represents the Mach number and Reynolds number at which for these tests the boundary layer will become transitional in the region of the corner.

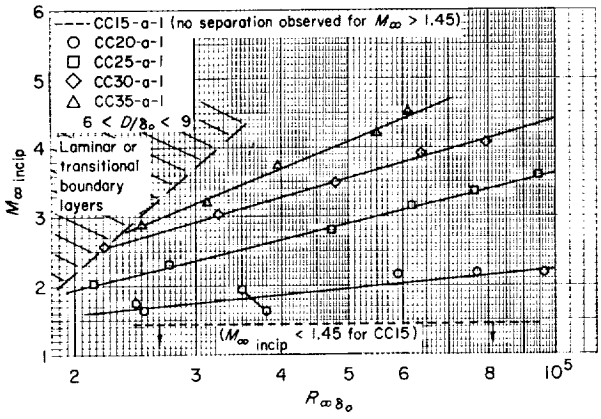

FIGURE 20.—Effect of Reynolds number on the Mach number for incipient separation for compression-corner flares.

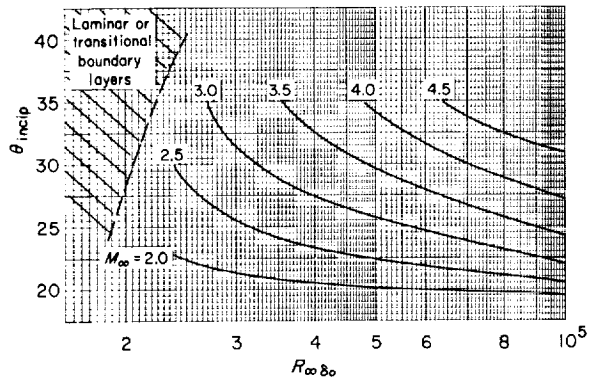

FIGURE 22.—Effect of Reynolds number on the flow-deflection angle for incipient separation for compression-corner flares.

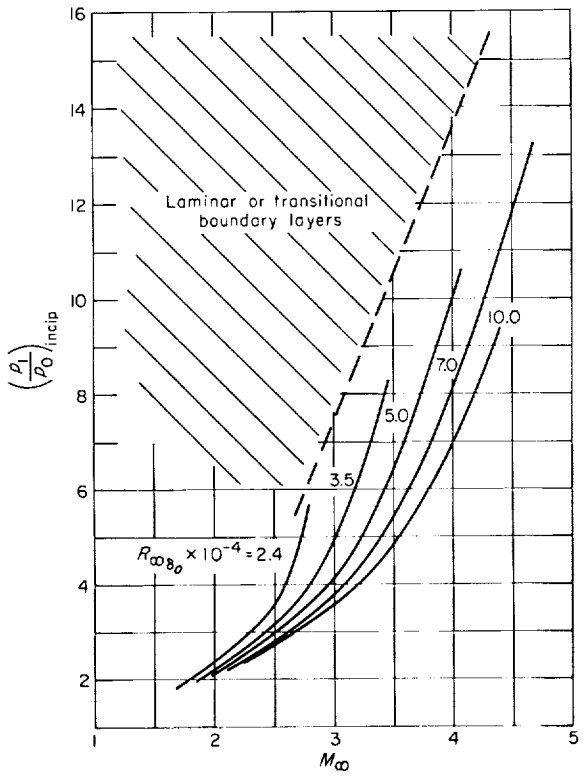

FIGURE 21.—Effect of Mach number on the pressure rise for incipient separation for compression-corner flares.

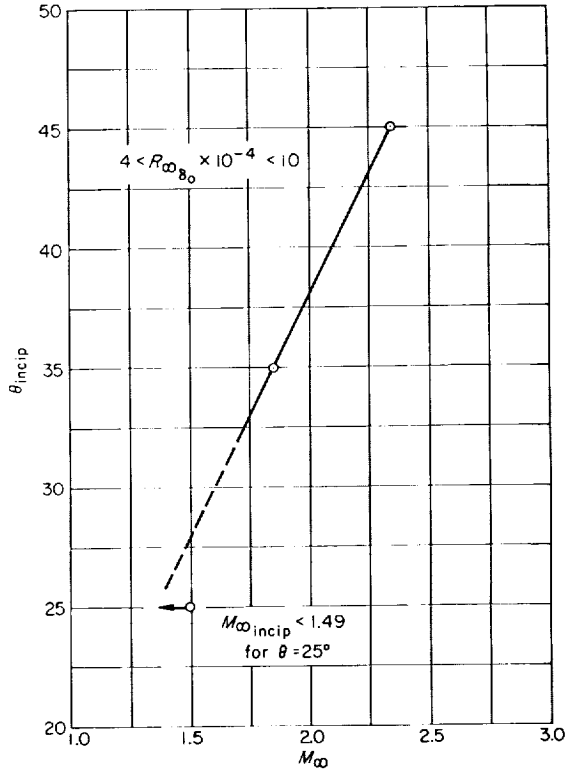

FIGURE 23.—Effect of Mach number on the maximum flare angle with no separation for curved-surface flares.

Flare angle is often a more convenient quantity than pressure rise for defining conditions for incipient separation because, for a given configuration, flare angle is constant, whereas over-all pressure rise varies with Mach number. The flare angle for incipient separation, obtained by cross-plotting the basic separation data, is shown in figure 22 as a function of Reynolds number and Mach number. Flares with angles greater than those represented by a particular curve will experience boundary-layer separation. The boundary layer will be attached for deflection angles less than the incipient values. Shown also in figure 22 is the maximum flare angle for which attached

flow is possible at the compression-corner flare under present test conditions regardless of Mach number and Reynolds number. This limit has been discussed previously. In the lower Reynolds number range and/or the higher Mach number range, Reynolds number has an important influence on the maximum flow-deflection angle possible with no boundary-layer separation.

Curved-surface flares. Flares with curved surfaces were investigated to determine the test conditions for which boundary-layer separation could be expected. A curved surface with a 2.6D radius was used with each of three flare angles (see fig. 1(b)). The effect of Mach number on the maximum possible flare angle with no separation for the curved flare is shown in figure 23. The data points shown for the 35° and 45° curved surfaces represent the minimum Mach numbers at which these flares could be tested with no separation. The boundary layer was attached to the 25° flare at Mach numbers down to the minimum possible for the test facility, with this model installation. The Mach number for incipient separation for the 25° curved surface (if separation does occur) will, therefore, be less than 1.49, as indicated in figure 23. The boundary layer was always separated for Mach numbers less than, or for values of flare angle greater than, those represented by the curve. The incipient-separation conditions for the curved flares were independent of Reynolds number. A possible reason for this is that the Mach number at which separation occurred was near that for which shock detachment would occur on a cone with angle equal to the flare angle. It is possible, therefore, that separation for the large-angle, curved-surface flares was triggered by the conditions for shock detachment, thus obscuring any possible effect of Reynolds number. Because of the hysteresis shown in figure 19, boundary-layer separation can also occur, under certain conditions, for Mach numbers greater than those represented by the curve. The magnitude of this hysteresis is dependent on Reynolds number.

COMPARISON OF TWO-DIMENSIONAL AND THREE-DIMENSIONAL BOUNDARY-LAYER SEPARATION

The data of this investigation for three-dimensional models are compared with the data of reference 12 for two-dimensional models to determine whether similarities exist in the separation phenomena. A long cylinder was, therefore, chosen so that the nose would be a sufficient distance from the flare. Thus, the nose had no effect on the flow in the region of the flare as shown by the negligible pressure gradient on the cylinder (fig. 15(a)) and by the negligible effect of changing nose shape on the first occurrence of flare-induced separation (figs. 15(b) and 15(c)). Approximately equal values of δ_0 on both the two- and three-dimensional models were also assumed desirable for this comparison. (In the course of the investigation, however, the actual boundary-layer thickness was observed to be relatively unimportant if Reynolds number was based on δ_0.) Since the three-dimensional model was much longer than the two-dimensional model, a smaller boundary-layer trip was dictated. Reasonably close agreement in δ_0 was attained when a 0.020-inch wire trip was placed well back on the cylinder to take advantage of the small growth of the laminar boundary-layer ahead of the trip. All data used in this comparison are for boundary layers with fully developed velocity profiles. (See fig. 13.)

COMPRESSION CORNERS

The separation phenomena were qualitatively the same for the two-dimensional and three-dimensional compression corners. Quantitatively, however, the incipient-separation conditions for the two-dimensional and three-dimensional compression corners were the same only for certain Mach numbers and Reynolds numbers. Figure 24(a) presents a comparison based on deflection angle. Undoubtedly a portion of this difference results because the pressure rise associated with a two-dimensional corner is larger than that for a three-dimensional corner for a given deflection angle. This, of course, suggests a comparison on the basis of pressure rise. Figure 24(b) shows that pressure rise is a better means for comparing two-dimensional and three-dimensional data than is deflection angle. Differences still exist, however, which depend on Mach number and Reynolds number. Figure 25 shows the Mach number and Reynolds number combinations for which the incipient-separation pressure ratios were similar for two- and three-dimensional models and the test conditions for which the incipient-separation pressure ratio of the three-dimensional model was

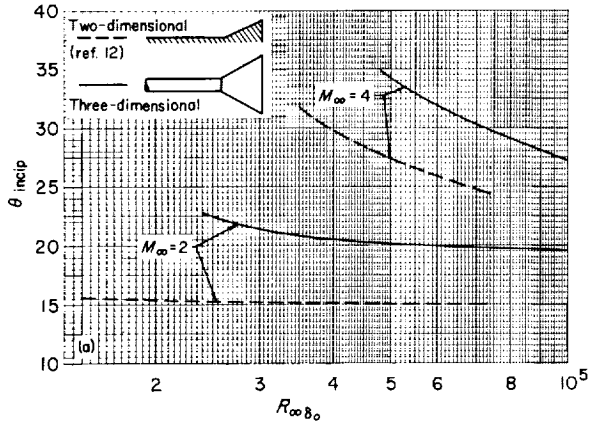

(a) Maximum flow-deflection angle with no separation.

FIGURE 24.—Comparison of incipient separation for a two-dimensional compression corner and a body of revolution with a compression-corner flare.

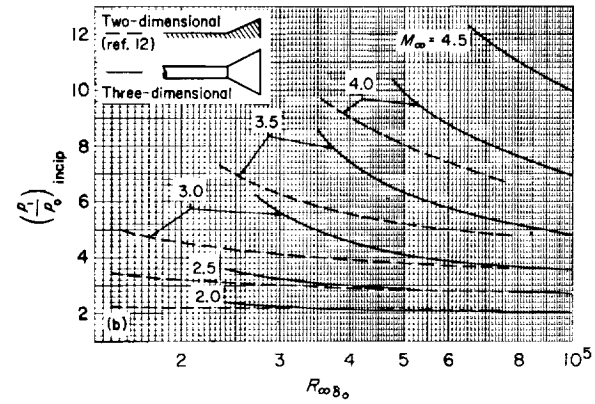

(b) Maximum pressure rise with no separation.

FIGURE 24.—Concluded.

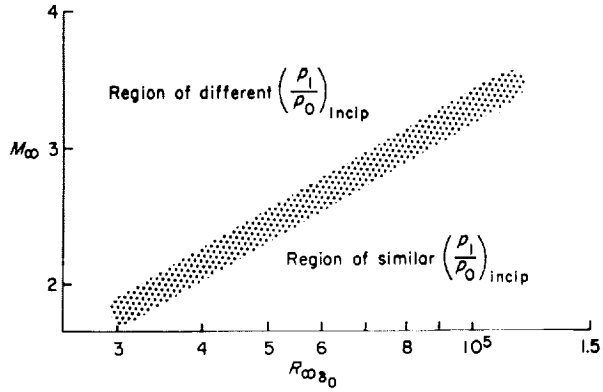

FIGURE 25.—Region of test conditions for which the two-dimensional and three-dimensional incipient separation pressure ratios are similar for compression corners.

greater than that for the two-dimensional model. The division of these two regions is approximate. In figure 12 it is indicated that D/δ_0 could explain at least some of the difference in incipient conditions for the two- and three-dimensional bodies. However, since D/δ_0 was essentially constant for the three-dimensional data in figure 24 (within a few percent for a given Mach number and within ± 15 percent over the entire Mach number range), the reason for the difference is not known.

CURVED SURFACES

Again, as for the compression corners, the flow separation on the three-dimensional curved surfaces was qualitatively similar to that on the two-dimensional curved surfaces. Quantitatively, however, the magnitude of the maximum pressure rise was greater for the three-dimensional curved surface than for the two-dimensional curved surface. It is interesting to note that the pressure rise for shock detachment for a cone is also higher than the corresponding pressure rise for a two-dimensional corner. This again suggests a possible relationship between the condition for shock detachment and the condition for incipient separation for the curved-surface models with large radii.

CONCLUSIONS

The following conclusions result from the investigation of turbulent boundary-layer separation on a cylinder-flare body of revolution in supersonic flow and from comparison of these three-dimensional data with the two-dimensional data of reference 12:

1. A decrease in the tendency toward boundary-layer separation resulted for both three-dimensional and two-dimensional models as Mach number was increased, or as Reynolds number, pressure rise or pressure gradient was decreased, with the exception that Reynolds number was unimportant to the incipient separation phenomena for the curved surfaces with the largest radii.

2. The pressure rise required for incipient boundary-layer separation for the three-dimensional compression surface was similar to that of the two-dimensional compression surface in the low Mach number and high Reynolds number ranges, and higher in the high Mach number and low Reynolds number ranges.

3. Cylinder-flare configurations with large ratios of cylinder diameter to boundary-layer thickness were more prone to boundary-layer separation than configurations with small ratios.

4. Heat flow into the model slightly reduced the extent of boundary-layer separation. This influence was consistent throughout the Mach and Reynolds number ranges considered.

5. The Mach number at which flare-induced boundary-layer separation first occured at a given Reynolds number was not affected by changing the nose shape, unit Reynolds number, the mode of promoting transition, or cylinder length if the Reynolds number was based on the thickness of a fully developed turbulent boundary layer.

6. Flare-induced pressure distributions for blunt- and sharp-nosed cylinders correlate on the basis of boundary-layer-edge conditions in the region of the corner. The final pressure attained on the flare correlates better on the basis of free-stream conditions.

7. Flare-induced separation of a fully developed turbulent boundary layer on a blunt-nosed cylinder can be predicted from data for sharp-nosed cylinders.

8. Boundary layers which did not have fully developed velocity profiles were more prone to boundary-layer separation than those with fully developed profiles.

AMES RESEARCH CENTER
NATIONAL AERONAUTICS AND SPACE ADMINISTRATION
MOFFETT FIELD, CALIF., *May 23, 1961*

REFERENCES

1. Chapman, Dean R. Kuehn, Donald M., and Larson, Howard K.: Investigation of Separated Flows in Supersonic and Subsonic Streams With Emphasis on the Effect of Transition. NACA Rep. 1356, 1958.
2. Bogdonoff, S. M., and Solaraki, A. H.: A Preliminary Investigation of a Shockwave-Turbulent Boundary Layer Interaction. Princeton Univ. Rep. 184, Nov. 1951.
3. Bogdonoff, S. M., Kepler, C. F., and San Lorenzo, E.: A Study of Shock-Wave Turbulent Boundary Layer Interaction at M=3. Princeton Univ. Rep. 222, July 1953.
4. Lange, Roy H.: Present Status of Information Relative to the Prediction of Shock-Induced Boundary-Layer Separation. NACA TN 3065, 1954.
5. Love, Eugene S.: Pressure Rise Associated With Shock-Induced Boundary-Layer Separation. NACA TN 3601, 1955.
6. Gadd, G. E.: Interactions Between Wholly Laminar or Wholly Turbulent Boundary Layers and Shock Waves Strong Enough to Cause Separation. Jour. Aero. Sci., vol. 20, no. 11, Nov. 1953, pp. 729–739.
7. Bogdonoff, S. M., and Kepler, C. E.: Separation of a Supersonic Turbulent Boundary Layer. Princeton Univ. Rep. 249, Jan. 1954.
8. Gadd, G. E., Holder, D. W., and Regan, J. D.: An Experimental Investigation of the Interaction Between Shock Waves and Boundary Layers. Proc. Roy. Soc. of London, ser. A., vol. 226, 1954, pp. 227–253.
9. Tyler, Robert D., and Shapiro, Ascher H.: Pressure Rise Required for Separation in Interaction Between Turbulent Boundary Layer and Shock Wave. Jour. Aero. Sci., vol. 20, no. 12, Dec. 1953, pp. 858 860.
10. Chapman, Dean R., Kuehn, Donald M., and Larson, Howard K.: Preliminary Report on a Study of Separated Flows in Supersonic and Subsonic Streams. NACA RM A55L14, 1956.
11. Bogdonoff, S. M.: Some Experimental Studies of the Separation of Supersonic Turbulent Boundary Layers. Papers presented at the Heat Transfer and Fluid Mechanics Institute, Univ. of Calif. at Los Angeles, June 23–25, 1955, sec. V, pp. 1–23.
12. Kuehn, Donald M.: Experimental Investigation of the Pressure Rise Required for the Incipient Separation of Turbulent Boundary Layers in Two-Dimensional Supersonic Flow. NASA MEMO 1–21–59A, 1959.
13. Migotsky, E., and Morkovin, M. V.: Three-Dimensional Shock-Wave Reflections. Jour. Aero. Sci., vol. 18, no. 7, July 1951, pp. 484–489.
14. Morkovin, M. V., Migotsky, E., Bailey, H. F., and Phinney, R. E.: Experiments on Interaction of Shock Waves and Cylindrical Bodies at Supersonic Speeds. Jour. Aero. Sci., vol. 19, no. 4, April 1952, pp. 237–248.
15. Crocco, Luigi, and Lees, Lester: A Mixing Theory for the Interaction Between Dissipative Flows and Nearly Isentropic Streams. Jour. Aero. Sci., vol. 19, no. 10, Oct. 1952, pp. 649–676.
16. Gadd, G. E.: An Experimental Investigation of Heat Transfer Effects on Boundary Layer Separation in Supersonic Flow. Jour. Fluid. Mech., vol. 2, part 2, Mar. 1957, pp. 105–122.

U.S. GOVERNMENT PRINTING OFFICE: 1962

NASA TR R-117
National Aeronautics and Space Administration.
TURBULENT BOUNDARY-LAYER SEPARATION INDUCED BY FLARES ON CYLINDERS AT ZERO ANGLE OF ATTACK. By Donald M. Kuehn. 1961. i, 26 p. diagrs., photo. GPO price 40 cents. (NASA TECHNICAL REPORT R-117)

Separation caused by the pressure rise induced by flares has been experimentally investigated in the Mach number range of 1.5 to 5.0 and in the Reynolds number range (based on boundary-layer thickness) of 1.5×10^4 to $12\times10.^4$ The purpose of the investigation was to determine the model geometry and flow conditions for which separation can be expected for a turbulent boundary layer of zero pressure gradient on the cylinder approaching the flare. Comparisons are made of the boundary-layer-separation characteristics of these three-dimensional flares with two-dimensional separation results from a previous investigation.

(Initial NASA distribution: 1, Aerodynamics, aircraft; 2, Aerodynamics, missiles and space vehicles; 20, Fluid mechanics.)

Copies obtainable from Supt. of Docs., GPO, Washington

I. Kuehn, Donald M.
II. NASA TR R-117

NASA

NASA TR R-117
National Aeronautics and Space Administration.
TURBULENT BOUNDARY-LAYER SEPARATION INDUCED BY FLARES ON CYLINDERS AT ZERO ANGLE OF ATTACK. By Donald M. Kuehn. 1961. i, 26 p. diagrs., photo. GPO price 40 cents. (NASA TECHNICAL REPORT R-117)

Separation caused by the pressure rise induced by flares has been experimentally investigated in the Mach number range of 1.5 to 5.0 and in the Reynolds number range (based on boundary-layer thickness) of 1.5×10^4 to $12\times10.^4$ The purpose of the investigation was to determine the model geometry and flow conditions for which separation can be expected for a turbulent boundary layer of zero pressure gradient on the cylinder approaching the flare. Comparisons are made of the boundary-layer-separation characteristics of these three-dimensional flares with two-dimensional separation results from a previous investigation.

(Initial NASA distribution: 1. Aerodynamics, aircraft; 2. Aerodynamics, missiles and space vehicles; 20, Fluid mechanics.)

Copies obtainable from Supt. of Docs., GPO, Washington

I. Kuehn, Donald M.
II. NASA TR R-117

NASA

NASA TR R-117
National Aeronautics and Space Administration.
TURBULENT BOUNDARY-LAYER SEPARATION INDUCED BY FLARES ON CYLINDERS AT ZERO ANGLE OF ATTACK. By Donald M. Kuehn. 1961. i, 26 p. diagrs., photo. GPO price 40 cents. (NASA TECHNICAL REPORT R-117)

Separation caused by the pressure rise induced by flares has been experimentally investigated in the Mach number range of 1.5 to 5.0 and in the Reynolds number range (based on boundary-layer thickness) of 1.5×10^4 to $12\times10.^4$ The purpose of the investigation was to determine the model geometry and flow conditions for which separation can be expected for a turbulent boundary layer of zero pressure gradient on the cylinder approaching the flare. Comparisons are made of the boundary-layer-separation characteristics of these three-dimensional flares with two-dimensional separation results from a previous investigation.

(Initial NASA distribution: 1, Aerodynamics, aircraft; 2, Aerodynamics, missiles and space vehicles; 20, Fluid mechanics.)

Copies obtainable from Supt. of Docs., GPO, Washington

I. Kuehn, Donald M.
II. NASA TR R-117

NASA

NASA TR R-117
National Aeronautics and Space Administration.
TURBULENT BOUNDARY-LAYER SEPARATION INDUCED BY FLARES ON CYLINDERS AT ZERO ANGLE OF ATTACK. By Donald M. Kuehn. 1961. i 26 p. diagrs., photo. GPO price 40 cents. (NASA TECHNICAL REPORT R-117)

Separation caused by the pressure rise induced by flares has been experimentally investigated in the Mach number range of 1.5 to 5.0 and in the Reynolds number range (based on boundary-layer thickness) of 1.5×10^4 to $12\times10.^4$ The purpose of the investigation was to determine the model geometry and flow conditions for which separation can be expected for a turbulent boundary layer of zero pressure gradient on the cylinder approaching the flare. Comparisons are made of the boundary-layer-separation characteristics of these three-dimensional flares with two-dimensional separation results from a previous investigation.

(Initial NASA distribution: 1, Aerodynamics, aircraft; 2, Aerodynamics, missiles and space vehicles; 20, Fluid mechanics.)

Copies obtainable from Supt. of Docs., GPO, Washington

I. Kuehn, Donald M.
II. NASA TR R-117

NASA